Analyzing Remote Sensing-Derived Normal Difference Vegetation Index to Predict Coastal Protection by *Spartina alterniflora*

by

Samantha C. Garber

B.S. Ocean Engineering, United States Naval Academy, 2022

Submitted to the Department of Mechanical Engineering in partial fulfillment of the requirements for the degree of

MASTER OF SCIENCE IN MECHANICAL ENGINEERING

jointly by

MASSACHUSETTS INSTITUTE OF TECHNOLOGY

and

WOODS HOLE OCEANOGRAPHIC INSTITUTION

September 2024

Authored by: Samantha Chan Garber
Department of Mechanical Engineering
August 9, 2024

Certified by: Heidi M. Nepf
Professor of Civil and Environmental Engineering, Thesis Supervisor

Accepted by: Alexandra Techet
Chair, Joint Committee for Applied Ocean Science and Engineering

Accepted by: Nicolas Hadjiconstantinou
Chairman
Graduate Officer, Department of Mechanical Engineering

Analyzing Remote Sensing-Derived Normal Difference Vegetation Index to Predict Coastal Protection by *Spartina alterniflora*

by

Samantha C. Garber

B.S. Ocean Engineering, United States Naval Academy, 2022

Submitted to the Department of Mechanical Engineering in partial fulfillment of the requirements for the degree of

MASTER OF SCIENCE IN MECHANICAL ENGINEERING

ABSTRACT

Coastal vegetation can provide protection to the coastline through its root structures, which reduce soil erosion, and its stem structures, which dissipate wave energy. The drag a plant induces could be used to quantify the amount of coastal protection that is provided. This study combined field measurements and drone surveys to develop methods for quantifying vegetation drag, focusing on Spartina alterniflora (*S. alterniflora*), a smooth cordgrass native to the study site: Waquoit Bay National Estuarine Research Reserve. The drag of a single plant is proportional to frontal area. The drag per bed area is proportional to the drag of a single plant and the number of stems per bed area. This study collected plant samples over the growing season to generate allometric relationships between tiller height and individual plant biomass and frontal area, which provides a way to translate remotely-sensed measures of biomass into stem count and frontal area per bed area. The frontal area was measured through digital imaging of individual plants. The elastic modulus of the stem was also measured using an Instron testing machine. For sixteen 1m x 1m test plots, Normalized Difference Vegetation Index (NDVI) extracted from drone multispectral imagery was compared to measured stem count and estimated biomass. The study compared two different years and three time points within a growing season [August 2022; June, August, October 2023]. In addition, at three plots the stem count was manually altered by cutting out 50% and 100% of the plants. This study found that while NDVI can be used to determine the abundance of *S. alterniflora*, there are several limitations that cause the correlations to be case-specific. Limitations to NDVI-*S. alterniflora* correlations included: (1) saturation, (2) species inhomogeneity of the area tested, (3) shoot density inhomogeneity of the area tested, and (4) environmental conditions.

Thesis supervisor: Heidi M. Nepf

Title: Professor of Civil and Environmental Engineering

Acknowledgements

First, I would like to thank my research advisor Dr. Heidi Nepf for her assistance and support throughout my studies. Next, I would like to extend many thanks to the Dr. Megan Tyrrell for her coordination and help in conducting field work at Waquoit Bay National Estuarine Research Reserve. Additionally, I would like to thank the groups and individuals whom supported and helped in field work to include Ernie Lee, Hyoungchul Park, Rachel Schaefer, James Brice, Trinity Stallins, Yuan Xu, Sal Netherton, Stephen Rudolph, Carolina Bastidas, Thomas van Veelen, Tansy Remiszewski, Theo Collins, Juliet Simpson, Autumn Deitrick, Damario Berry, Divine Siam, and the Massachusetts Department of Transportation. Lastly, I would like to thank my family and my husband for their support during my studies.

Contents

1 Introduction

1.1 Purpose

The purpose of this study was to evaluate the use of Normalized Difference Vegetation Index to quantify the abundance of coastal vegetation, specifically *Spartina alterniflora*. However, the study revealed several limitations of this method including species and shoot density homogeneity and environmental conditions.

1.2 Motivation

The motivation of quantifying vegetation density using a remote sensing is that this method allows for quicker, less labor-intensive measuring than a manual method. Remote sensing also allows for less disruption and damage to the flora and fauna observed as there is no foot traffic in the area studied.

1.3 Site and Species of Interest

1.3.1 Site: Waquoit Bay

This study was conducted at Waquoit Bay National Estuarian Research Reserve (WBNERR). Waquoit Bay is located on the southern shore of Cape Cod, MA. Fig. 1 is a Google Satellite view of Waquoit Bay.

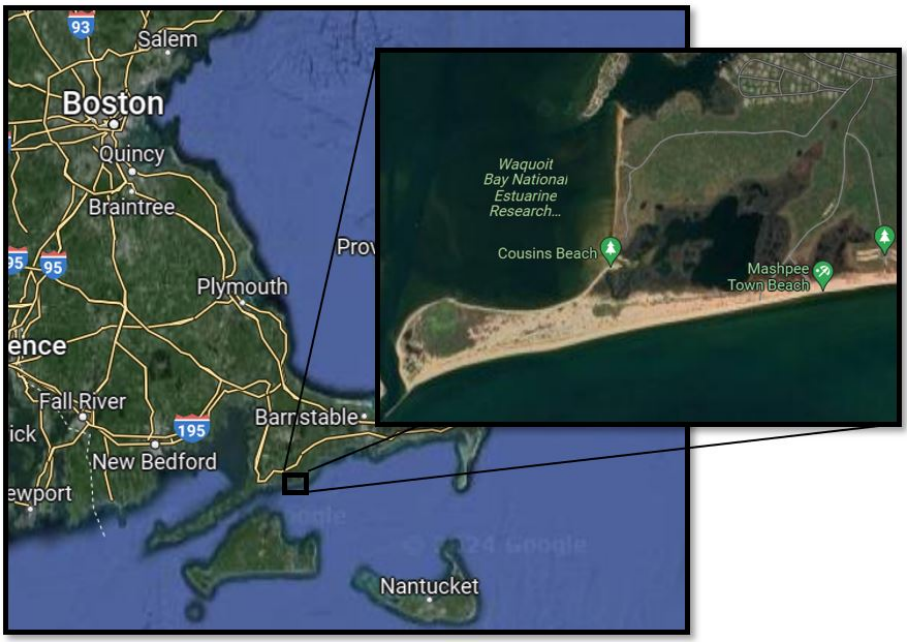

Figure 1: Google Satellite View of Waquoit Bay

1.3.2 Species: *Spartina alterniflora*

Spartina alterniflora (S. alterniflora) **is a native, smooth cordgrass along the eastern shore of the United States.** ***S. alterniflora*** **can be found in marshes with brackish or salt water (Native Plant Trust, n.d.). The typical height of** ***S. alterniflora*** **ranges from 0.6 to 1.8m (Materne et al., 2022).** ***S. alterniflora*** **can be characterized as having a main stem, starting at the soil line, and depending on the maturity having multiple leaves and flowers.** ***S. alterniflora*** **is found in abundance in Waquoit Bay. Fig. 2 is an image of a sample of** ***S. alterniflora*** **collected during this study.**

Figure 2: *S. alterniflora* Sample

1.4 Normalized Difference Vegetation Index

The vegetation index of interest, to quantify the abundance of ***S. alterniflora*****, in this study was Normalized Difference Vegetation Index (NDVI). NDVI is commonly used in agriculture as a means to monitor the crop abundance and fitness (Team Cropin, n.d.). Defined by Equation (1), NDVI is a ratio of near-infrared (NIR) and red light bands.**

$$\text{NDVI} = \frac{\text{NIR} - \text{Red}}{\text{NIR} + \text{Red}} \tag{1}$$

NIR light is reflected by mesophyll cells and red light is absorbed by chlorophyll (EUMeTrain, 2010). Greater NIR light reflection and red light absportion is associated with healthier vegetation (USGS, n.d.). NDVI has been used in previous studies to map and quantify the abundance of ***S. alterniflora*** **(Liu et al., 2020; Nardin, 2021). NDVI ranges from -1.0 to 1.0, in which negative values indicate water and clouds; values near zero**

indicate bare soil; and positive values indicate vegetation (USDA, n.d.). Values between 0.1 and 0.5 suggest sparse vegetation and values 0.6 and greater suggest dense vegetation (USDA, n.d.).

1.5 Duration of Study

This study was conducted over two growing seasons: August 2022; June, August, and October 2023.

2 Allometric Relationships

Allometric relationships of *S. alterniflora* structure and rigidity were created using samples from Waquoit bay in August 2022 and June, August, and October 2023. The allometric relationships created were:

1. Diameter versus Tiller Height
2. Vegetation Volume versus Tiller Height
3. Biomass versus Tiller Height
4. Frontal Area versus Tiller Height
5. Rigidity versus Tiller Height

The purpose for determining the diameter of a single *S. alterniflora* plant is to calculate the volume and rigidity of a single plant. The purpose for determining the vegetation volume and biomass serve as methods for characterizing vegetation abundance. The purpose for determining the frontal area of a single plant is to calculate the drag force, F, on a single plant.

For rigid plants, the drag induced by a single plant is

$$F_R = \frac{1}{2} C_D A U^2 \tag{2}$$

in which, F_R is the drag force on a single rigid plant, C_D is the drag coefficient, A is the frontal area, and U is a steady current or wave velocity.

The purpose for determining the rigidity of a single plant is because if a plant is flexible, the drag decreases because the frontal area is decreased due to the plant bending. Bending causes the plant to become more streamline thus reducing the relative velocity due to part of the plant moving with the wave.

Shown in Equation (3), the Cauchy number describes the ratio of hydrodynamic drag to plant rigidity.

$$Ca = \frac{1}{2} \frac{\rho C_D A U^2 L^2}{EI} \tag{3}$$

in which, L is the tiller height, E is Young's modulus of the plant stem, and I is the bending moment of inertia of the plant stem shown in Equation (4).

$$I = \frac{\pi D^4}{64} \tag{4}$$

in which, D is the diameter of the *S. alterniflora* stem.

This study assumed that the vegetation is subjected to a current, U, that bends the plant in a 2-D reconfiguration. Luhar and Nepf (2011) found if $Ca < 1$, then the plant will not bend. However, if $Ca > 1$, then the plant will exhibit bending in one plane which yields Equation (5).

$$\frac{F}{F_R} = Ca^{-\frac{1}{3}} \tag{5}$$

in which, F is the drag force with reconfiguration and F_R is the drag force of a single rigid plant.

The drag per bed area of a marsh is

$$\frac{Drag}{BedArea} = m(\frac{1}{2}C_D A U^2)Ca^{-\frac{1}{3}} \tag{6}$$

in which, m is the stem count per bed area of the marsh.

2.1 Methodology

2.1.1 Diameter

The following diameter analysis was conducted on August 2022 samples of ***S. alterniflora*** collected from Waquoit Bay. The tiller height was measured, using a meter stick, while the sample was in the ground. The diameter was measured, using a digital caliper, near tiller base for each sample.

2.1.2 Volume

The following volume analysis was conducted on August 2022 samples of ***S. alterniflora*** collected from Waquoit Bay to determine the volume of all S. alterniflora plants per bed area. The tiller height and diameter were measured using the diameter protocol above. The plot density was provided by WQNEER and used for stem counts.

2.1.3 Biomass

The following biomass analysis was conducted on the combined August 2022 and June, August, and October 2023 samples of ***S. alterniflora*** collected from Waquoit Bay.

In August 2022, two samples from each plot were harvested, then measured for the tiller height, and weighed. The first sample of each plot represented a smaller specimen and the second sample represented a larger specimen. In June 2023, 7 samples total were randomly selected from the plots and were measured for tiller height before harvesting, then harvested, and weighed. In August and October 2023 , 8 and 10 samples, respectively, total were randomly selected and followed the same protocol as June 2023. For all four sampling dates, the samples were placed in a paper bag, labeled, put in an oven, taken out of the paper bag, and weighed once a day. Once the

sample's change in weight was less than 5%, the sample was considered at its dry weight.

2.1.4 Frontal Area

The following frontal area analysis was conducted on August 2022 samples of *S. alterniflora* collected from Waquoit Bay. The *S. alterniflora* samples were placed individually on a plain, white background. A studio light was placed directly overhead of the samples to light the sample without introducing shadows. Then, an image was taken of each sample and the image was cropped so that the sample was fully in the image with minimal background to prevent error of shadows. MatLab was used to determine the number of pixels per plant which was converted to area measured in cm^2 per plant. Fig. 3 is an example of one of the *S. alterniflora* sample images used.

Figure 3: *S. alterniflora* Sample

2.1.5 Rigidity

The following rigidity analysis was conducted on August 2022 samples of *S. alterniflora* collected from Waquoit Bay. Two samples from each plot were harvested. The central stem of each sample was identified and was de-leafed. The diameter of the sample at the point that the Instron came into contact with the sample was measured. The minimum sample length of $6cm$ was determined based on the testing span of the Instron so that there was overhang and the sample did not fall out when deflection began. The testing span, labeled as the horizontal distance from A to B in Fig. 4a with length $4cm$, of the Instron was determined based on test samples to allow maximum

deflection of the samples without the samples falling out of the Instron. The force in N, measured using the Bluehill Universal Instron Application, was confirmed to be 0 and then the Instron was moved so the machine just began touching the sample. At this point, the displacement was zeroed. Each sample was run until a displacement of $8mm$ was met. This condition was determined based on three sample runs where the thickest part of a main ***S. alterniflora*** stem was used as the test samples. The Young's modulus of each sample was calculated using the proportional limit, which is the end of the linear slope portion, of the force-displacement curve produced by the Instron as shown in Fig. 4b.

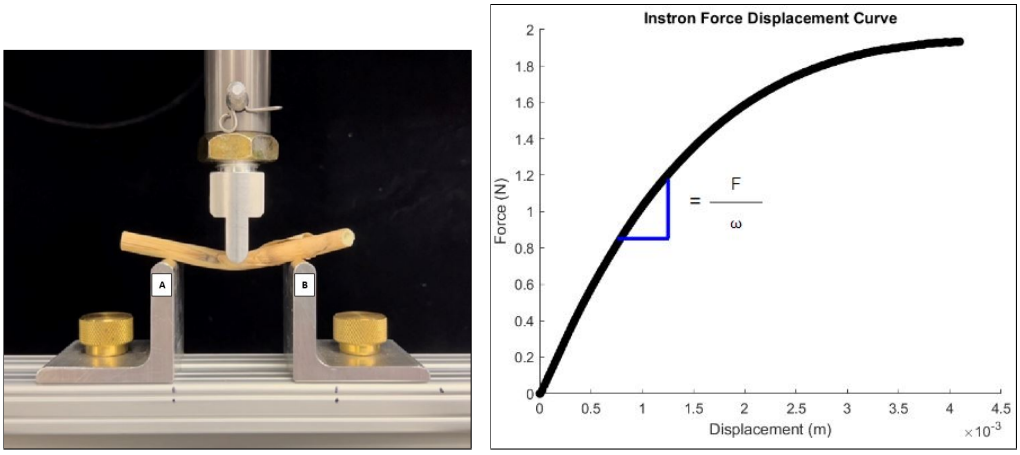

(a) *S. alterniflora* Sample Subjected to 3-Point Bending Test

(b) Example of Force Displacement Curve Produced by the Instron

Figure 4: Instron Test and Curve

The three-point bending test can be modeled as a simply supported beam with a center load. The deflection, ω, of the ***S. alterniflora*** sample is located at the center load and is directly related to the rigidity of the sample as shown in Equation (7).

$$\omega = \frac{Fl^3}{48EI} \tag{7}$$

in which, F is the load in N, and l is the testing span in m. Equation (7) was rearranged to solve for the rigidity of each sample as shown in Equation (8).

$$\text{Rigidity} = EI = \frac{F}{\omega}\frac{l^3}{48} \tag{8}$$

in which $\frac{F}{\omega}$ is the slope of the linear portion of the force-displacement curve.

2.2 Diameter

Fig. 5 is a plot of the August 2022 sampled ***S. alterniflora*** diameter versus tiller height.

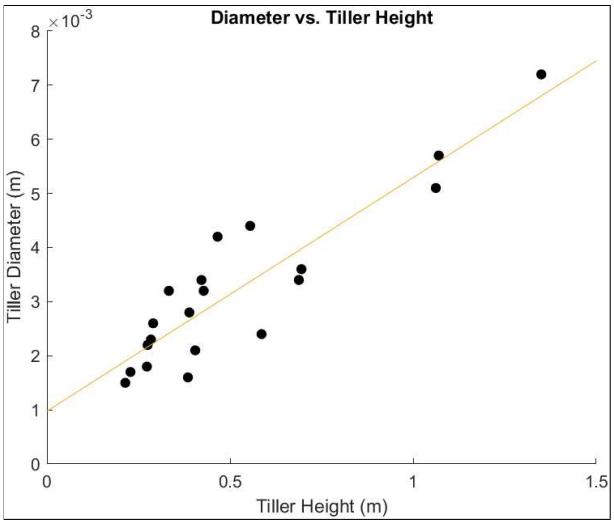

Figure 5: *S. alterniflora* Diameter vs. Tiller Height

As shown in Fig. 5, there was a positive correlation between diameter and tiller height. A linear regression with 95% confidence interval was conducted resulting in Equation (9).

$$D = (0.0043 \pm 0.0005)L + (0.0010 \pm 0.0003) \tag{9}$$

in which D is the diameter for a single plant in m, and L is tiller height in m.

2.3 Volume

The diameter, determined using Equation (9), could then be used to determine the volume of *S. alterniflora* per bed area. Nardin (2021) calculated vegetation volume of *S. alterniflora* using Equation (10) and assumed a single, central stem without leaves.

$$V_n = m * D * L \tag{10}$$

in which V_n is the vegetation volume calculated using Nardin's (2021) method.

This study modified Nardin's (2021) vegetation volume equation from 2-D to 3-D, due to the *S. alterniflora* central stem commonly seen as cylindrical shaped, as shown in Equation (11).

$$V = m * L * \pi(\frac{D}{2})^2 \tag{11}$$

As with Nardin (2021), this study assumed a single, central stem without leaves. The reason for assuming a single, central stem is to simplify the structure of *S. alterniflora*. However, it is acknowledged that the additional volume provided by leaves is not negligible. Liu et al. (2022) found, for the approximate latitude of Waquoit Bay at 41.6 degrees, the mean *S. alterniflora* leaf area is 25cm^2 and mean *S. alterniflora* leaf thickness is 30mm. If the volume of a single leaf is calculated as its area multiplied by its thickness, the volume of a single *S. alterniflora* leaf for Waquoit Bay is 0.000075m^3. The mean number of leaves per *S. alterniflora* plant collected in August 2022 was 6. Assuming each leaf has a volume of 0.000075m^3, the total volume of leaves per *S. alterniflora* plant is 0.00045m^3. The mean volume of a single, central stem calculated from *S. alterniflora* samples collected during August 2022 was 0.00000774m^3. The ratio of volume of leaves to a single stem is 58:1. Due to the large difference between volume of leaves and volume of a single stem, neglecting the leaves and modeling the *S. alterniflora* as a single, central stem when determining the total plant volume is inaccurate.

2.4 Biomass

Fig. 6 is a plot of the August 2022 and June, August, and October 2023 sampled *S. alterniflora* ln(biomass) versus ln(tiller height).

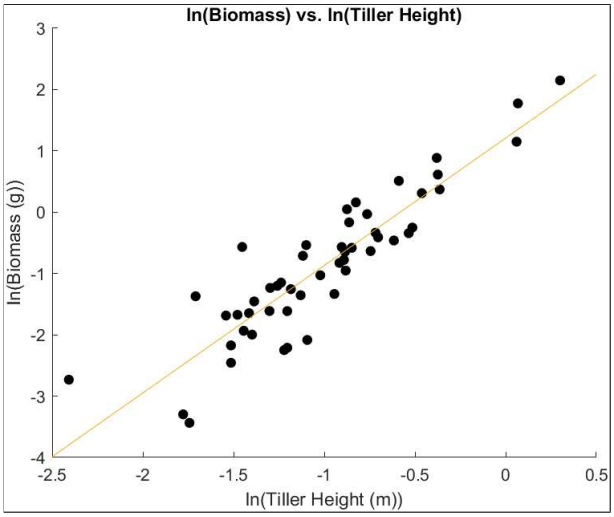

Figure 6: *S. alterniflora* Biomass vs. Tiller Height (Raw Data Located in Tables 8, 10, 12, and 14)

A log-log regression analysis was conducted on the biomass and tiller height data since a linear relationship, shown as Equation (12), best fit the transformed data.

$$ln(B) = (2.1 \pm 0.1) * ln(L) + (1.2 \pm 0.2) \quad (12)$$

in which B is biomass for a single plant in g, and L is the tiller height in m. This relationship can be used to determine the biomass of ***S. alterniflora*** if the tiller height is known.

A linear relationship in log-log transformed data was also found by González Trilla et al. (2013) and Hill and Roberts (2017). González Trilla et al. (2013) found the biomass-tiller height relationship as Equation (13).

$$log(B_{GTrilla}) = 2.1log(H_{GTrilla}) - 3.1 \tag{13}$$

in which, $B_{GTrilla}$ is the biomass of a single stem and biomass of all the leaves on the stem in g, and $H_{GTrilla}$ is the tiller height in cm. Differences in the biomass-tiller height allometric equation found by González Trilla et al. (2013) could be attributed to the study site located in Argentina. Though the species studied by González Trilla et al. (2013) was ***S. alterniflora***, a different study site results in environmental differences such as temperature and resources available that would attribute to size variation of ***S. alterniflora*** (Crosby et al., 2017; Liu et al., 2022).

The biomass-tiller height relationship found during the months of June to August found by Hill and Roberts (2017) in seaward, open water surrounded, Louisiana locations are described in Equations (14) and (15).

$$log(B_{HR1}) = 1.9log(H_{HR1}) + 1.0 \tag{14}$$

$$log(B_{HR2}) = 1.4log(H_{HR2}) + 1.0 \tag{15}$$

in which, B_{HR1} is the biomass of a single stem and biomass of all the leaves on the stem in g located in Bay La Fleur, Louisiana; H_{HR1} is the tiller height in cm located in Bay La Fleur, Louisiana; B_{HR2} is the biomass of a single stem and biomass of all the leaves on the stem in g located in Lake Barre, Louisiana; and H_{HR2} is the tiller height in cm located in Lake Barre, Louisiana. Similar to González Trilla et al. (2013), Hill and Roberts (2017) had a different study site location than this study which could be the reason for coefficient and x-intercept differences in the biomass-tiller height allometric equation found.

The biomass and tiller height log-log regression calculated with a 95% confidence level. The ***S. alterniflora*** biomass and tiller height relationship was simplified to Equation (16):

$$B = (3.4 \pm 1) * L^{(2.1 \pm 0.1)} \tag{16}$$

Equation (17) combines Equation (16) and the stem count per 1 m^2 to determine the biomass per 1 m^2 bed area.

$$B_T = B * m \tag{17}$$

in which B_T is the biomass per 1 m^2 bed area in g/m^2.

2.5 Frontal Area

Fig. 7 is a plot of the August 2022 sampled *S. alterniflora* ln(frontal area) versus ln(tiller height).

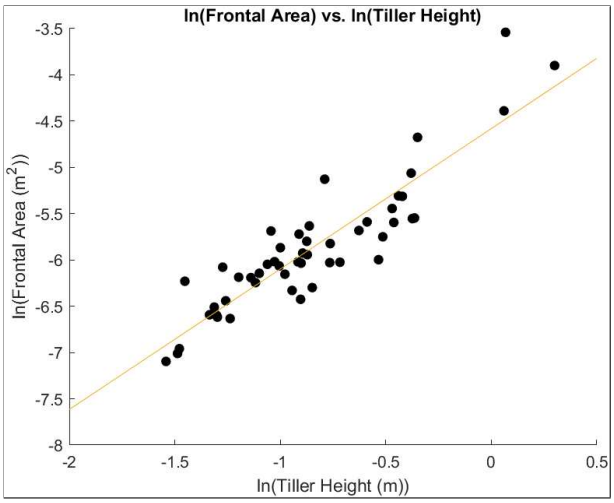

Figure 7: *S. alterniflora* Frontal Area vs. Tiller Height

A log-log regression analysis was conducted on the frontal area and tiller height data since a linear relationship, shown as Equation (18), best fit the transformed data.

$$ln(A) = (1.5 \pm 0.1) * ln(L) - (4.6 \pm 0.1) \tag{18}$$

in which A is the frontal area for a single plant in m^2, and L is the tiller height in m. This relationship could be used to determine the frontal area of *S. alterniflora* if the tiller height is known.

The frontal area and tiller height log-log regression calculated with a 95% confidence level. The *S. alterniflora* frontal area and tiller height relationship was simplified to Equation (19):

$$A = (0.010 \pm 1) * L^{(1.5 \pm 0.1)} \tag{19}$$

Equation (20) combines Equation (19) and the stem count per 1 m^2 to determine the frontal area per 1 m^2 bed area.

$$A_T = A * m \tag{20}$$

in which A_T is the frontal area per 1 m^2 bed area in m^2/m^2.

2.6 Rigidity

Fig. 8 is a plot of the August 2022 sampled *S. alterniflora* rigidity versus tiller height. Table 15 shows how the rigidity was calculated for the *S. alterniflora* samples.

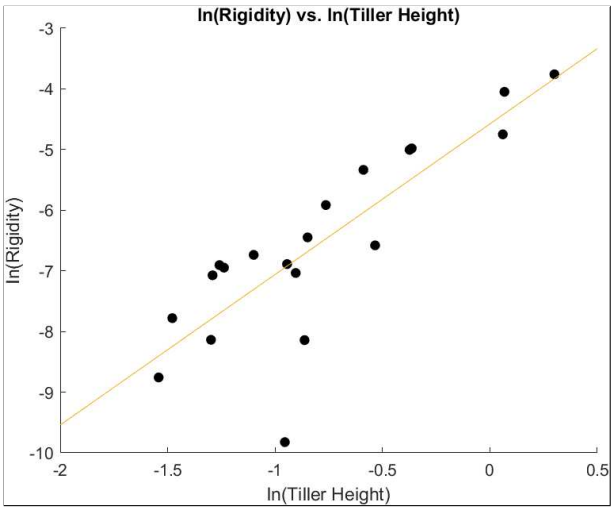

Figure 8: *S. alterniflora* Rigidity vs. Tiller Height

A log-log regression analysis was conducted on the rigidity and tiller height data since a linear relationship, shown as Equation (21), best fit the transformed data.

$$ln(EI) = (2.5 \pm 0.4) * ln(L) - (4.6 \pm 0.4) \tag{21}$$

in which EI is the rigidity for a single plant in Nm^2, and L is the tiller height in m. This relationship could be used to find the rigidity of *S. alterniflora* not measured as long as the tiller height is known.

The rigidity and tiller height log-log regression calculated with a 95% confidence level. The *S. alterniflora* rigidity and tiller height relationship was simplified to Equation (22):

$$EI = (0.010 \pm 0.01) * L^{(2.5 \pm 0.4)} \tag{22}$$

2.7 *Spartina patens (S. patens)* Relationships

***S. patens*, another common cordgrass found at Waquoit Bay, was sampled and tested using the same methods as conducted on *S. alterniflora*. There was no allometric relationship produced for diameter and tiller height due to no correlation and similar sizing of all samples. Therefore, the mean *S. patens* diameter sampled August 2022 was $D_P = 0.88 \pm 0.2mm$. The mean *S. patens* tiller height sampled August 2022 was $L_P = 24 \pm 2cm$. The *S. patens* allometric relationships produced are shown in Table 1.**

Measurement	Relationship
Volume	$V_P = m * L * \pi(\frac{D_P}{2})^2$
Biomass	$B_P = (0.00040 \pm 0.0003) * L_P^{(1.5 \pm 0.2)}$
Frontal Area	$A_P = (0.20 \pm 0.1) * L_P^{(0.99 \pm 0.3)}$

Table 1: *S. patens* Relationships

3 Protocol

3.1 Goals

The goals of the fieldwork conducted were to (1) create allometric relationships for the structure and abundance of *S. alterniflora* and (2) determine if there was a relationship between the abundance of *S. alterniflora* and NDVI.

3.2 Plots

3.2.1 WBNERR Plots

The vegetation plots studied in August 2022 were preexisting plots created by WBNERR. Fig. 9 is a map of Waquoit Bay, created by WBNERR, containing the section and plot locations. There were two different sections in Waquoit Bay: "Section 1" and "Section 2." Within each section, WBNERR created multiple transects perpendicular to the shoreline noted as "T1," "T2," and "T3" for both sections. Each transect contained multiple 1m by 1m vegetation plots noted as "P1," "P2," etc. The standard for naming each plot followed: "S"Section Number - Transect Number - Plot Number. In which, the plot number for each plot most seaward was 1 and increased numerically landward. Therefore, the most seaward plot located in section 2 and transect 3 would be S2-3-1. Each plot was designated using 4 PVC pipes at each corner as shown in Fig. 10.

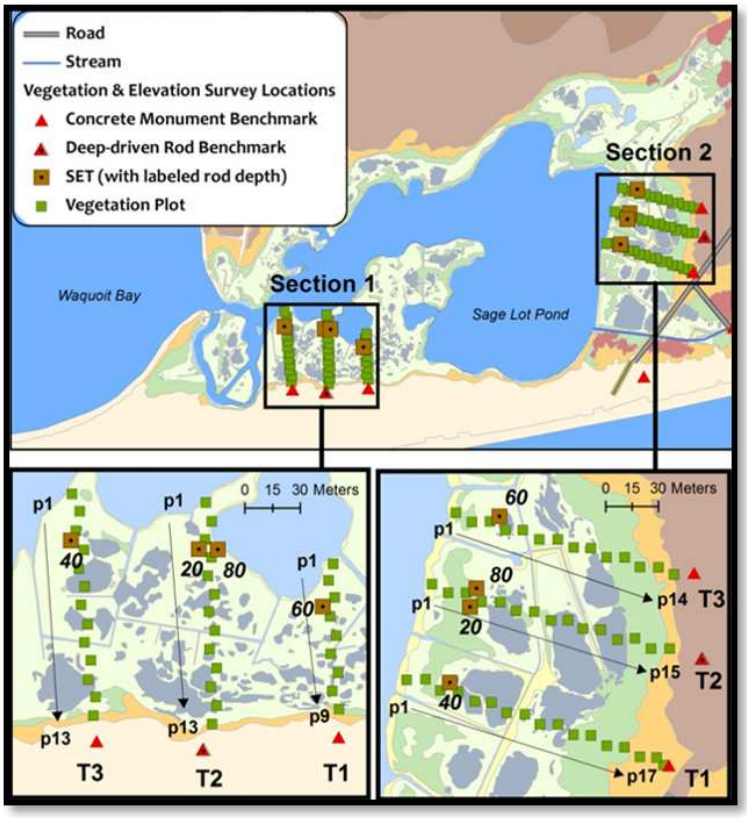

Figure 9: WBNERR Map of Waquoit Bay Sections, Transects, and Vegetation Plots

Figure 10: WBNERR Plot S2-2-13

3.2.2 Additional Plots Created

The vegetation plots studied in June, August, and October 2023 were created along the boardwalk of Section 2 in Waquoit Bay. Fig. 11 indicates the location of the boardwalk in Section 2. The reason plots were created along the preexisting boardwalk was to reduce the amount of damage to the marsh caused by foot traffic.

17 plots were created: 10 perpendicular to the shoreline and 7 parallel to the shoreline. The plots perpendicular to the shoreline were spaced approximately 8m apart. The plots parallel to the shoreline were spaced approximately 2m apart. Fig. 12 is a map of the plot layout along the boardwalk.

Figure 11: Location of Boardwalk in Section 2

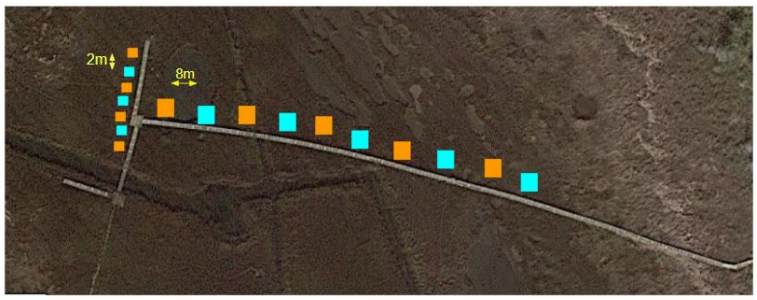

Figure 12: Plots Created Along Boardwalk in Section 2 of Waquoit Bay

Fig. 13 is a photograph of the boardwalk. As shown in Fig. 14, each plot measured 1m by 1m and was designated using 4 flags at each corner. Orange and blue flags were used to note even and odd plots, respectively.

Figure 13: Location of Boardwalk in Section 2

Figure 14: Example of 1 of 17 Plots (Plot 16)

Using the plot layout in Fig. 12, and a tape measure, the approximate location of each plot was found. Next, flags, of the same color, were placed at each corner of a plot where the distance between each flag was measured 1m apart using a meter stick. Using a Trimble1, the latitude and longitude of the center of each plot was recorded to an accuracy of 6 decimal places which is approximately 0.11m.

Section 2 was chosen as the location of interest for the plots studied in June, August, and October 2023 because: (1) the preexisting boardwalk minimized marsh damage caused by foot traffic, (2) Section 1 did not have a boardwalk, and (3) Section 2 had a greater abundance of areas with only *S. alterniflora*.

3.3 Drone Flights

In August 2022, the drone flight was conducted by the Massachusetts Department of Transportation (MassDOT) as shown in Fig. 15. Stitching together the images captured, MassDOT created a multispectral orthomosaic of Sections 1 and 2 of Waquoit Bay.

Figure 15: MassDOT Drone Flight

In June, August, and October 2023, the drone and cameras used were a Phantom 4 Pro with a Sentera Double 4K Multispectral attachment as shown in Fig. 16.

Figure 16: Phantom 4 Pro with Sentera Double 4K Multispectral Attachment

In June 2023, the flight was conducted using Sentera's FieldAgent Desktop and Mobile app. Prior to conducting fieldwork in June, the approximate latitude and longitude of each plot was found using Google Maps. The latitude and longitudes were imported into ArcGIS to create plot .shp files.

These files were then uploaded into the FieldAgent Desktop app to create each plot as a "Field." The FieldAgent Desktop and Mobile app were then cloud synced. For the flight, the FieldAgent Mobile app was used with the following flight parameters: flight altitude of 50 ft and overlap of 80%. The drone flew to each "Field" and took one photo. For June 2023, all images were imported into QGIS to manually calculate NDVI using QGIS' raster calculator. Each image contained a plot and had to first be corrected in order to calculate NDVI using the true band values.

Sentera's Double 4k Multispectral Sensor used two lenses, which contained different filters, to capture 5 bands: red, green, blue, near-infrared, and red edge. The first lens captured red, green, and blue. The second lens captured red edge, [garbage], near-infrared. The stacked filters in each lens cause each band channel to capture multiple bands. For example, the blue channel captured primarily blue wavelengths however there were contributions by red and green wavelengths. Therefore, the raw images had be corrected to find the true band values. Before the true band values could be calculated, the images were first georeferenced using Ground Control Points (GCPs) since the lenses did take photos simultaneously. This meant that if the two images were to be superimposed, to conduct raster calculations, the images were offset. The GCPs were the latitude and longitude of each plot corner captured by the Trimble1.

To calculate the true band values, the images were normalized, for total exposure opportunity, using the image's gain and shutter speed. The reason for this is that the shutter speed and gain of each image was not the same, meaning that the apparent brightness of the image would differ due to differing ISO and exposure times (FADGI, n.d.). The ISO refers to the camera's sensitivity to light and exposure time refers to the how long the camera is exposed to the light (Adobe, n.d. & ThermoFisher Scientific, n.d.). Equation (23) was used to calculate the gain of each image.

$$\text{Gain} = \frac{\text{ISO}}{100} \tag{23}$$

The ISO and shutter speed, in seconds, of each image was located in the image's metadata. Each image was imported into QGIS in which the raster calculator was used to normalize each image using Equation (24).

$$\text{Exposure Opportunity} = \frac{\text{DN}}{\text{Gain} * \text{Shutter Speed}} \tag{24}$$

In which, DN is the digital number of the band from the image. Finally, the true band values were calculated by importing each image into QGIS and using the raster calculator for each Equations (25), (26), (27), (28), and (29) provided by Sentera (Sentera Support, 2022).

$$\text{Blue} = 1.377 * \text{DNblue} - 0.182 * \text{DNGreen} - 0.061 * \text{DNRed} \tag{25}$$

$$\text{Green} = \text{-0.199*DNBlue} + 1.420 * \text{DNGreen} - 0.329 * \text{DNRed} \tag{26}$$

$$\text{Red} = -0.034 * \text{DNBlue} - 0.110 * \text{DNGreen} + 1.150 * \text{DNRed} \quad (27)$$

$$\text{Red Edge} = -0.956 * \text{DNBlue} + 1.000 * \text{DNRed} \quad (28)$$

$$\text{NIR} = 2.426 * \text{DNBlue} - 0.341 * \text{DNRed} \quad (29)$$

The true band values were then used to calculate the mean NDVI of each plot using Equation (30).

$$NDVI_{Sentera} = \frac{2.700 * \text{NIR} - \text{Red}}{2.700 * \text{NIR} + \text{Red}} \quad (30)$$

Equation (8) is different from Equation (refer to "normal NDVI equation" in background chapter) because Sentera's true band equations resulted in band normalization values which were a step increase in proper band range values of 0 to 255. Therefore, Equation (8) was used to correct Sentera's band math gains.

To increase efficiency and reduce the potential error introduced when manually correcting each photo, August and October 2023 drone flights were corrected using Pix4DMapper. In August 2023, flights were conducted using Sentera's FieldAgent Mobile app. A polygon mission was created around all of the plots and the boardwalk with the flight parameters being: flight altitude of 200 ft and overlap of 80%. The overlap remained the same from the June 2023 drone flight. The change in flight altitude, from the June 2023 to August 2023 drone mission, was due to Sentera's recommendation based on using Pix4DMapper to stitch together the images (Sentera Support, n.d.).

The procedure and parameters for the drone flights conducted October 2023 was the same as in August 2023 with one alteration: the polygon mission was only created around the Plots A and B.

3.4 Data Collected

3.4.1 Allometric Relationship Measurements

During the August 2022 fieldwork, the data collected were: tiller height, biomass, frontal area, diameter, and Young's Modulus. The procedures for the data collected used, with the exception of tiller height, were described in the Allometric Relationships chapter. The tiller height procedure for August 2022 differed from June, August, and October 2023 in that the tiller height was measured after the *S. alterniflora* was removed from the plot. The issue regarding the accuracy of this method is analyzed in the results.

During the June, August, and October 2023 fieldwork, the data collected were: tiller height, biomass, and stem counts. The tiller height and biomass procedures used were described in the Allometric Relationships chapter.

During August 2022 fieldwork, inaccuracy of tiller height measurement was conducted. The tiller height of a *S. alterniflora* was measured after the plant was removed from the plot. The plant was not necessarily always cut directly at the soil line, which resulted in a shorter tiller height being recorded. The tiller height measurement was then changed to measuring the *S. alterniflora* before removal for June, August, and October 2023. Due to this, the tiller height data collected during June, August, and October 2023 was used for the allometric relationships.

3.4.2 Stem Counts

The stem counts used in August 2022 were provided by WBNERR.

The stem counting method in June, August, and October 2023 was the same. Two sized quadrats were used to conduct stem counts: $0.25m$ by $0.25m$ and $0.5m$ by $0.5m$. The subplots of each quadrat were $0.083m$ by $0.083m$ and $0.1m$ by $0.1m$, respectively. Fig. 17 shows the layout of the $0.25m$ by $0.25m$ and $0.5m$ by $0.5m$ quadrat.

Q1	Q2	Q3
Q4	Q5	Q6
Q7	Q8	Q9

(a) $0.25m$ by $0.25m$ Quadrat

Q1	Q2	Q3	Q4	Q5
Q6	Q7	Q8	Q9	Q10
Q11	Q12	Q13	Q14	Q15
Q16	Q17	Q18	Q19	Q20
Q21	Q22	Q23	Q24	Q25

(b) $0.5m$ by $0.5m$ Quadrat

Figure 17: Quadrats Used for Stem Counts

To conduct stem counts, first, the quadrats were randomly placed in each plot. The size of quadrat used was recorded. For both quadrats, once placed in the plot, the tiller height of all the stems in the corner squares of the quadrat subplots were measured and recorded. Therefore, for the larger quadrat, Q1, Q5, Q21, and Q25 were used. Likewise, for the smaller quadrat, Q1, Q3, Q7, and Q9 were used.

The stem counts were recorded as either *S. alterniflora* stems per $0.027556m^2$ for the $0.25m$ by $0.25m$ quadrat or as *S. alterniflora* stems per $0.04m^2$ for the $0.5m$ by $0.5m$ quadrat. The stem counts recorded as stems per $0.027556m^2$ were then multiplied by 36.29 to determine the stem count per $1m^2$ which was the total area of each plot. Likewise, the stem counts recorded as stems per $0.04m^2$ were multiplied by 25 to determine the stem count per $1m^2$. Fig. 18 shows the stem counting method using the $0.25m$ by $0.25m$ and $0.5m$ by $0.5m$ quadrat.

(a) $0.25m$ by $0.25m$ Quadrat (b) $0.5m$ by $0.5m$ Quadrat

Figure 18: Stem Counting Method

3.4.3 Harvesting

S. alterniflora **harvesting was only conducted in August and October 2023. For this study, harvesting was defined as removing a known amount of *S. alterniflora*. For both August and October 2023, the harvested plots were from the plots created in June 2023 and chosen based on vegetation harvest approval from WBNERR.**

In August 2023, Plot 6 shown in Fig. 19, was the harvested plot. The remaining plots acted as controls. The blue squares in Fig. 19b represent the two $0.25m$ by $0.25m$ quadrats placed at corners B and D. The two quadrats note the locations of harvest between Flights 1 and 2. Flight 1 captured Plot 6 with 100% vegetation abundance. After Flight 1, 50% of the vegetation from both quadrats were removed reducing the total *S. alterniflora* plot abundance by 6%.

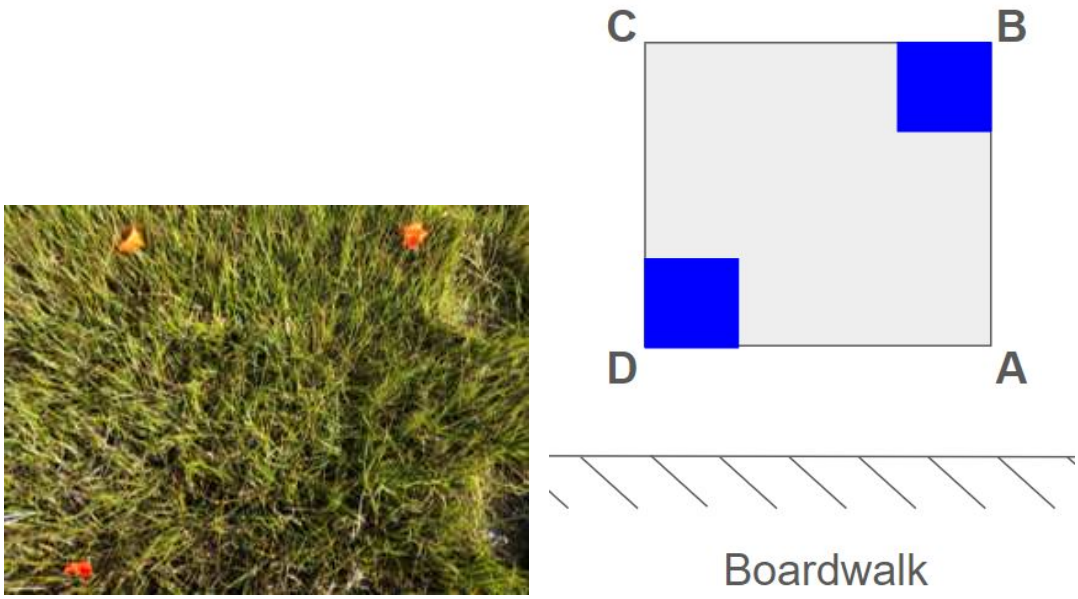

(a) Plot 6 before Harvesting

(b) Plot 6 Diagram

Figure 19: Plot 6

In October 2023, Plot 3 and Plot 5 referred to as Plot B and Plot A, respectively and shown in Fig. 20, were chosen chosen as the harvested plots. Within each plot, subplots were created as shown in Fig. 21 using $0.25m$ by $0.25m$ quadrats. A1, A2, B1, and B2 each represent the area of one quadrat while the controls in Plots A and B represent the area of two quadrats. For harvesting, after the 1st drone flight was conducted, 50% of the *S. alterniflora* plants were removed in subplots A1, A2, B1, and B2 were removed. After the 2nd drone flight was conducted, the remaining *S. alterniflora* in subplots A1, A2, B1, and B2 were removed.

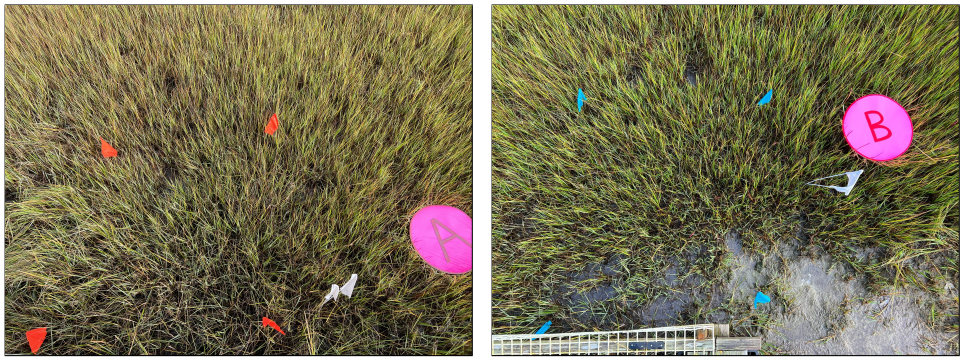

(a) Plot A

(b) Plot B

Figure 20: Plots A and B before Harvesting

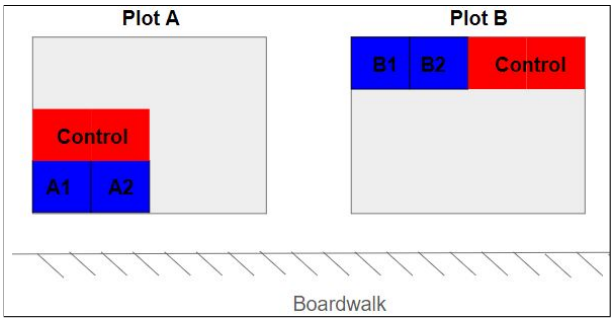

Figure 21: Plot A and Plot B Subplot Layout

4 Results

4.1 Multispectral Orthomosaics

In August 2022, the multispectral orthomosaics of Waquoit Bay created by MassDOT were analyzed to determine possible relationships between *S. alterniflora* abundance and NDVI. Fig. 22 contains the multispectral orthomosaics of Waquoit Bay's Section 1 and Section 2 captured and stitched by MassDOT. Orthomosaics are multiple images stitched together where each image was taken at a different time and location.

Both multispectral orthomosaics contain areas shaded darker than others due to sunlight intensity, sunlight position, and cloud cover. Variation in time and location attributes to different sunlight intensity and position captured by the sensor yielding darker or lighter image portions (NebGuide, 2017). Cloud cover contributes to darker portions captured by the sensor by casting shadows. During the August 2022 drone flight, the sky condition was scattered clouds as seen in Fig. 23.

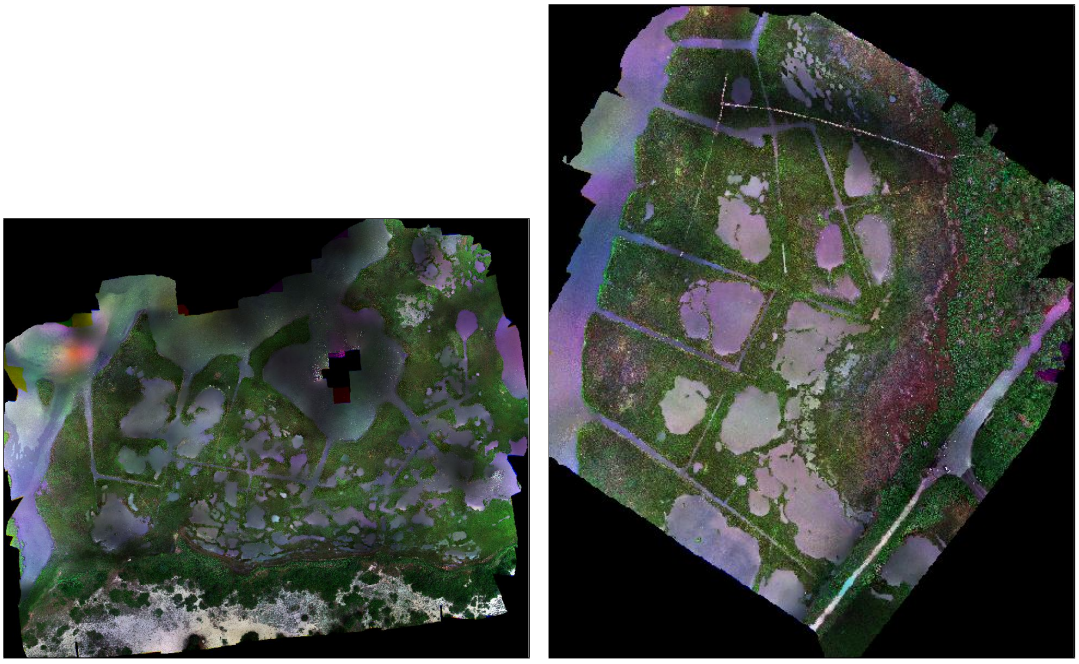

(a) Section 1 (b) Section 2

Figure 22: August 2022 Waquoit Bay Multispectral Orthomosaics

Figure 23: August 2022 Cloud Cover

4.2 RGB and NIR-RE Images

In June 2023, the RGB and NIR-RE images of each plot were analyzed to determine possible relationships between *S. alterniflora* abundance and NDVI. Fig. 24 contains an example of RGB and NIR-RE photos taken (Plot 7).

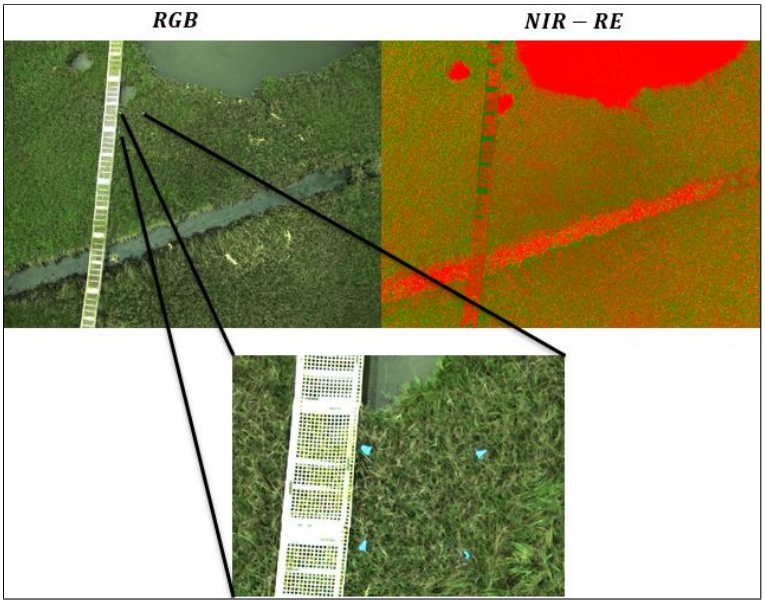

Figure 24: Individual RGB and NIR-RE Photos Taken of Plot 7

4.3 NDVI Orthomosaics

In August and October 2023, NDVI orthomosaics were created by importing the RGB and NIR-RE images captured by the drone into Pix4DMapper.

The NDVI orthomosaics were analyzed to determine possible relationships between *S. alterniflora* abundance and NDVI.

Fig. 25 contains the NDVI orthomosaics of August 2023's Flight 1 and 2.

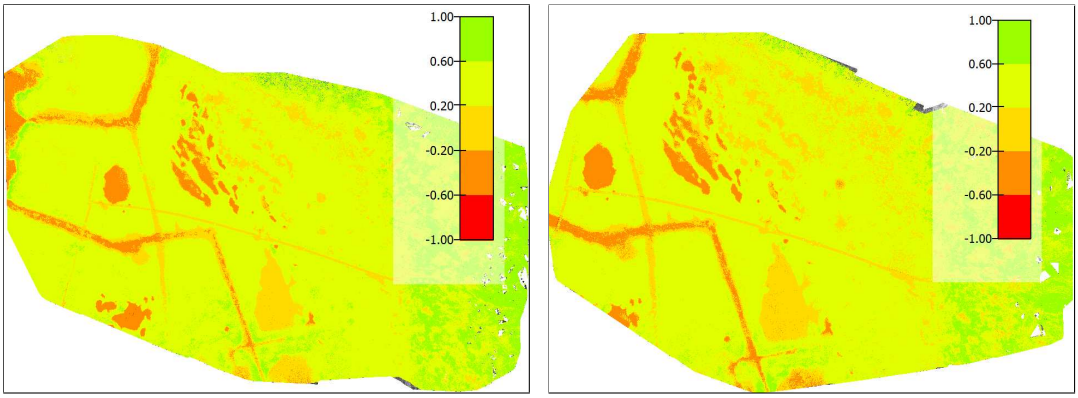

(a) Flight 1 (b) Flight 2

Figure 25: August 2023 NDVI Orthomosaics

Fig. 26 contains the NDVI orthomosaics of October 2023's Flight 1, 2, and 3.

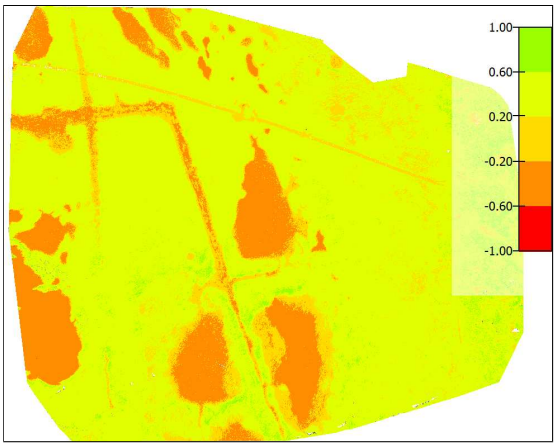

(a) Flight 1

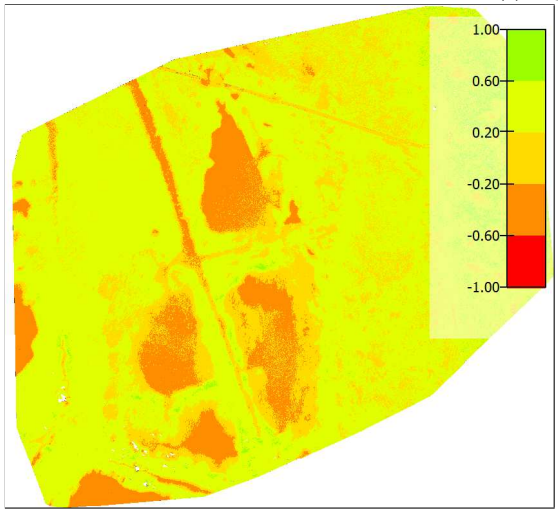

(b) Flight 2

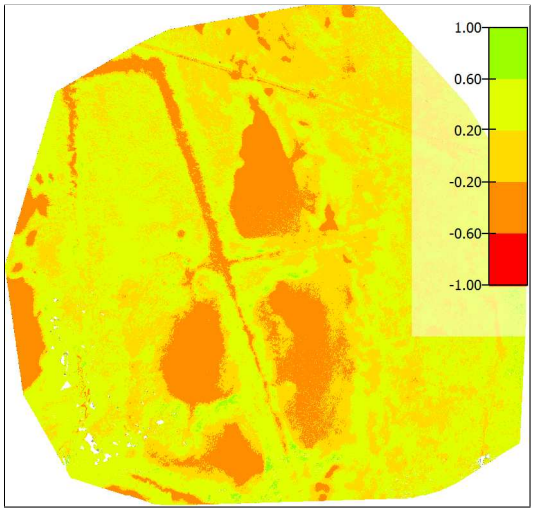

(c) Flight 3

Figure 26: October 2023 NDVI Orthomosaics

4.4 Vegetation Abundance and NDVI

In August 2022, June 2023, and August 2023, the possible relationship between vegetation abundance and NDVI was explored using vegetation abundance in the form of: vegetation volume, biomass, and stem count. The vegetation volume, biomass, and stem count of each plot was calculated using the allometric relationships created from plants collected from the site. In October 2023, the possible relationship between vegetation abundance and NDVI was explored using vegetation abundance in the form of stem count.

Figs. 27, 28, and 29 show the NDVI of each plot versus different methods of vegetation abundance of each plot for August 2022.

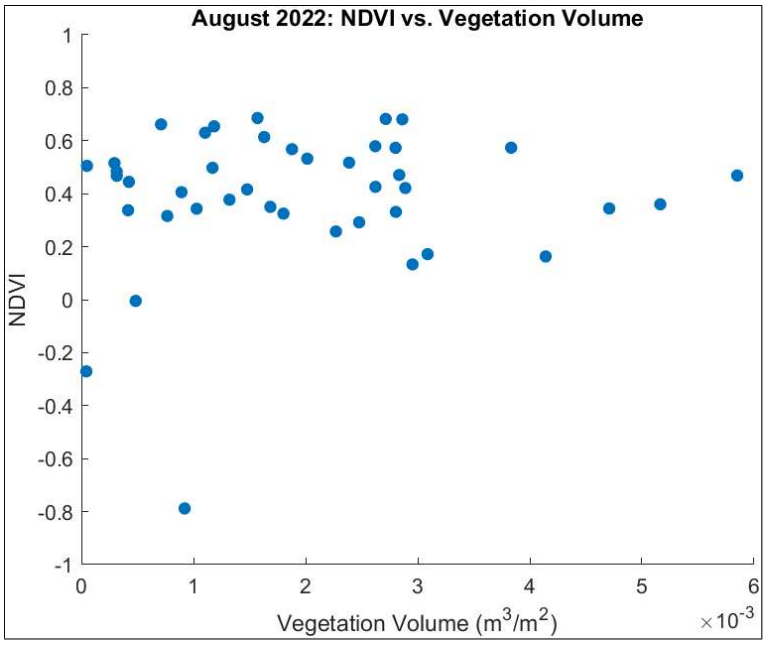

Figure 27: NDVI vs. Vegetation Volume (V)

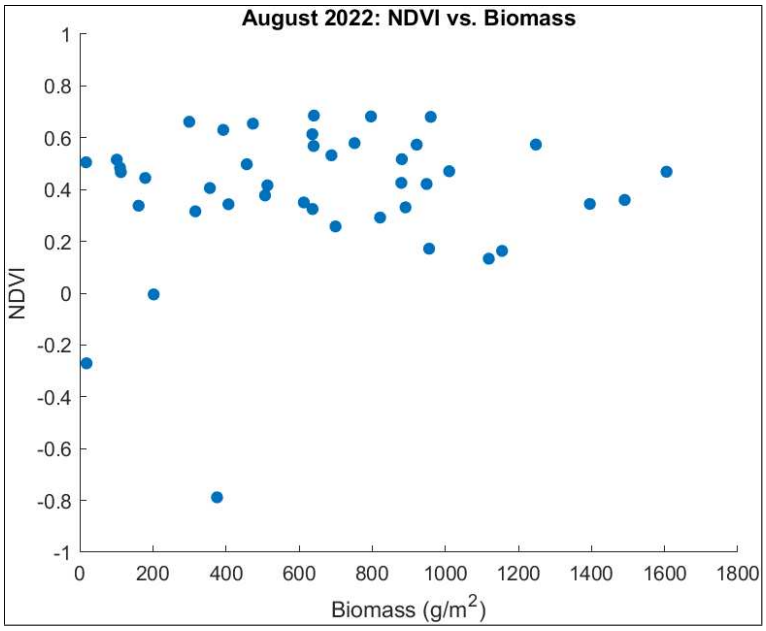

Figure 28: NDVI vs. Biomass (B)

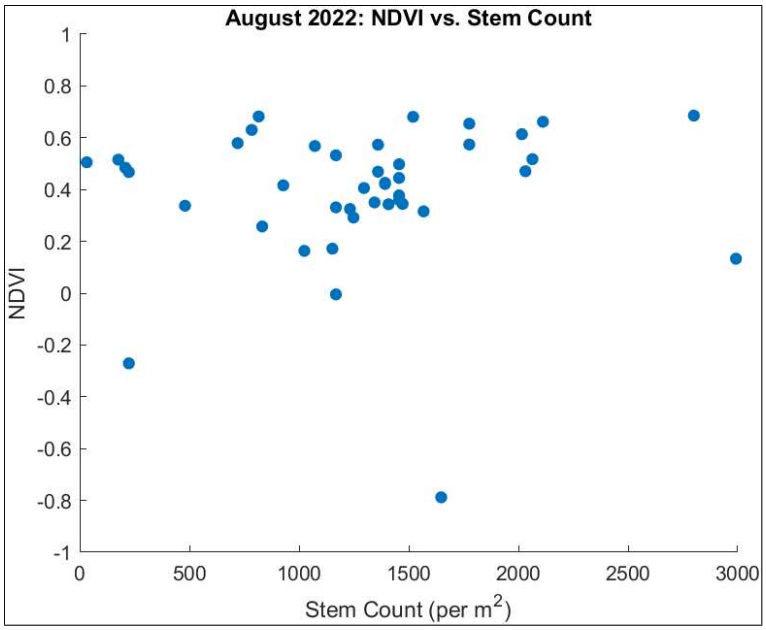

Figure 29: NDVI vs. Stem Count (m)

A linear regression was conducted on Figs. 27, 28, and 29. The linear regression for Figs. 27, 28, and 29 are shown in Equations (31), (32), and (33), respectively.

$$\text{NDVI} = (16 \pm 20)V + (0.34 \pm 0.05) \tag{31}$$

$$\text{NDVI} = (-0.000057 \pm 0.00007)B + (0.34 \pm 0.05) \tag{32}$$

$$\text{NDVI} = (-0.0000042 \pm 0.00004)m + (0.37 \pm 0.06) \tag{33}$$

Within uncertainty, the slopes of Figs. 27, 28, and 29 are zero which indicates there is no correlation between NDVI and vegetation abundance. The reason for there being no relationship could be the issue of (1) saturation, (2) species inhomogeneity, and/or (3) shoot density inhomogeneity.

Saturation could be the issue because there could be a threshold in which an increase in *S. alterniflora* abundance would not change the NDVI measured. To determine if saturation was the issue, a threshold analysis was conducted on August 2023 data. If there was a correlation between *S. alterniflora* abundance and NDVI in August 2023 in the threshold analysis, then the issue for no correlation in August 2022 between *S. alterniflora* abundance and NDVI was due to saturation.

Species inhomogeneity could be the issue because though the plots studied in August 2022 were *S. alterniflora* dominated, other species were present. The other species included in calculating the mean NDVI of each plot could have contributed to a different measured NDVI than if the plot measured only had *S. alterniflora* resulting in no correlation between NDVI and vegetation abundance. To determine if species inhomogeneity was the issue,

plots studied in June, August, and October 2023 only contained *S. alterniflora*. If there were a correlation between *S. alterniflora* abundance and NDVI in June, August, and October 2023, then the issue for no correlation in August 2022 between *S. alterniflora* abundance and NDVI was due to multiple species present.

Shoot density inhomogeneity could be the issue because the stem count in a subarea of a plot might not be representative of the entire plot. Therefore, extrapolating the stem count of a subarea to an entire plot would be inaccurate. To determine if shoot density inhomogeneity was the issue, all of the stems in subplots studied in October 2023 were counted. If there was a correlation between *S. alterniflora* abundance and NDVI in October 2023, then the issue for no correlation in August 2022 between *S. alterniflora* abundance and NDVI was due to shoot density inhomogeneity.

In June 2023, the mean NDVI of each plot was calculated using the same method as in August 2022 except instead of using a multispectral orthomosaic, the georeferenced RGB and NIR-RE images were imported into QGIS. Figs. 30, 31, and 32 show the NDVI of each plot versus different methods of vegetation abundance of each plot for June 2023.

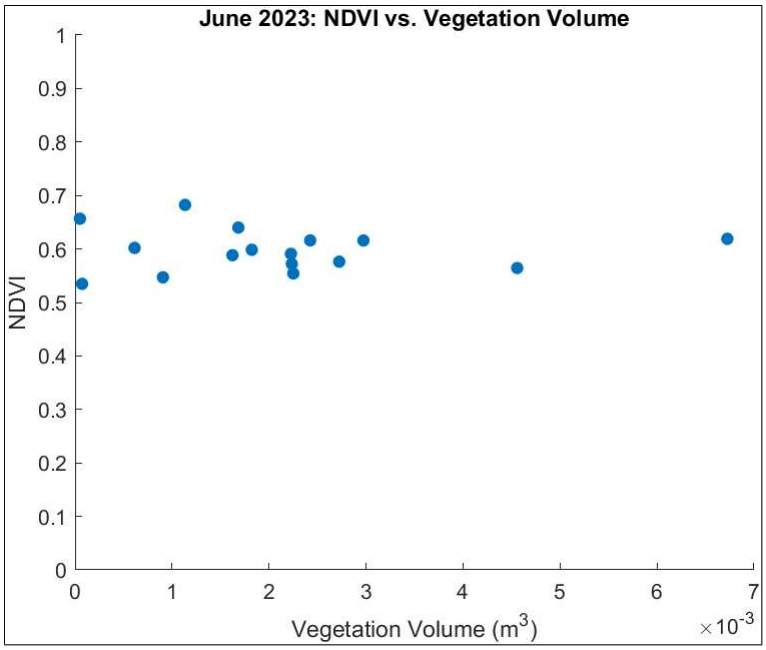

Figure 30: NDVI vs. Vegetation Volume (V)

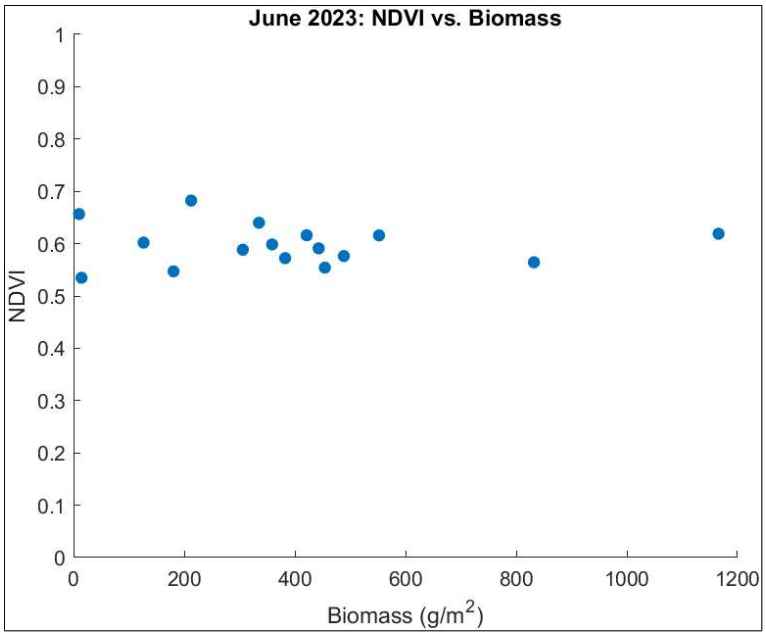

Figure 31: NDVI vs. Biomass (B)

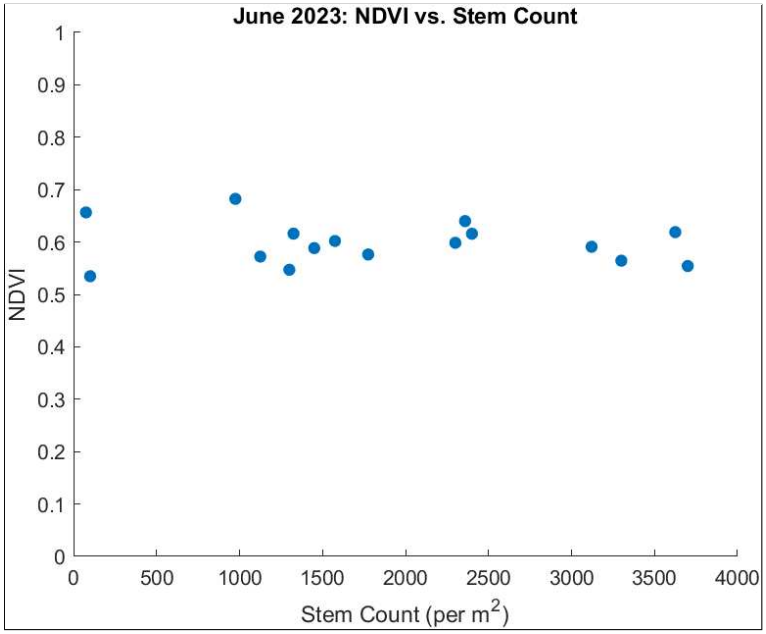

Figure 32: NDVI vs. Stem Count (m)

A linear regression was conducted on Figs. 30, 31, and 32. The linear regression for Figs. 30, 31, and 32 are shown in Equations (34), (35), and (36), respectively.

$$\text{NDVI} = (-0 \pm 6)V + (0.60 \pm 0.02) \tag{34}$$

$$\text{NDVI} = (-0.0000044 \pm 0.00004)B + (0.60 \pm 0.02) \tag{35}$$

$$\text{NDVI} = (-0.0000049 \pm 0.000009)m + (0.61 \pm 0.02) \tag{36}$$

Within uncertainty, the slopes of Figs. 30, 31, and 32 are zero which indicates there is no correlation between NDVI and vegetation abundance. The multiple steps in correcting the photos could have introduced errors which could explain the lack of relationship between NDVI and vegetation abundance. The fieldwork images taken by the drone in August and October 2023 were corrected using Pix4DMapper to eliminate the multiple steps required to correct the photos to confirm whether or not that was the reason for the lack of relationship.

For the same point in the growing season, Nardin (2021) had a NDVI range of approximately 0.4 to 0.7 and a vegetation volume of 180,000 to 380,000mm^3. The vegetation volume found by Nardin (2021) was smaller by a factor of 10 than the data captured during June 2023. The difference in vegetation abundance could be attributed to different locations of study and the size range of *S. alterniflora* (Native Plant Trust, n.d.). The NDVI range for June 2023 was within, and narrower, that Nardin's (2021) NDVI range. However, within the range, Nardin (2021) saw a positive correlation between NDVI and vegetation abundance. This suggests that this relationship can only be seen for smaller vegetation abundances and there is a limit where any more increase in vegetation abundance results in the saturation of NDVI.

The mean NDVI for August 2023's Flights 1 and 2 were compared for each plot. The mean NDVI should not drastically vary for the plots since none of the plots, except for Plot 6, were harvested. It is important to note that during Flights 1 and 2, none of the plots were inundated. Fig. 33 shows the difference in mean NDVI calculated for plots during Flights 1 and 2.

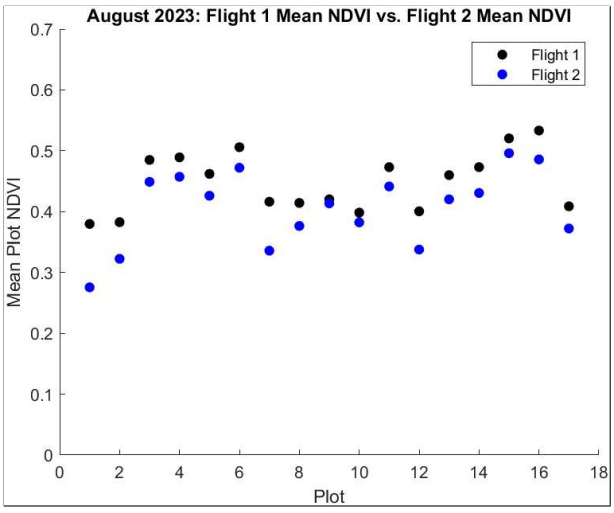

Figure 33: August 2023: Flight 1 (12:00 PM EDT) Mean Plot NDVI vs. Flight 2 (1:30 PM) Mean Plot NDVI (Plot 6 was harvested)

From the difference between Flight 1 and Flight 2's NDVI calculated, a coefficient, Beta, was calculated with:

$$\text{Beta} = \text{mean of all control plots}(\frac{NDVI_2}{NDVI_1}) = 0.899 \tag{37}$$

This suggests that between Flight 1 and Flight 2, the change between NDVI calculated was approximately 11%. This difference could describe the reason for some of the difference between Plot 6's variation in mean NDVI for the flights. While all of the plots were not inundated, and the control plots did not have the biomass altered, the reason for a difference between NDVI calculated in Flights 1 and 2 could be attributed to a difference in the position of the sun. The flights were conducted approximately 1.5 hours apart.

To further explore the relationship between NDVI and vegetation abundance, Flight 1 of August 2023 was analyzed since the flight occurred at similar environmental conditions, of sun position and tide level, as August 2022 and June 2023. Flight 1 of August 2022, June 2023, and August 2023 occurred at low tide and approximately an hour before high noon. High noon is characterized as occurring at 12:00 PM standard time and the point at which the sun is at its highest position in the sky (Cambridge University Press, n.d.). All flights occurred during daylight savings time. The difference in sun position between Flight 1 and Flight 2 can be determined using the solar hour angle which is the change in the sun's position east or west of the local meridian (Bhatia, 2014). Flight 1 occurred at 12:00 PM daylight savings time which means that the hour angle is -15°. Flight 2 occurred at 1:30 PM daylight savings time, 1.5 hours after 12:00 PM, which means that the hour angle is +7.5°.

Figs. 34, 35, and 36 show the NDVI of each plot versus different methods of vegetation abundance of each plot for August 2023.

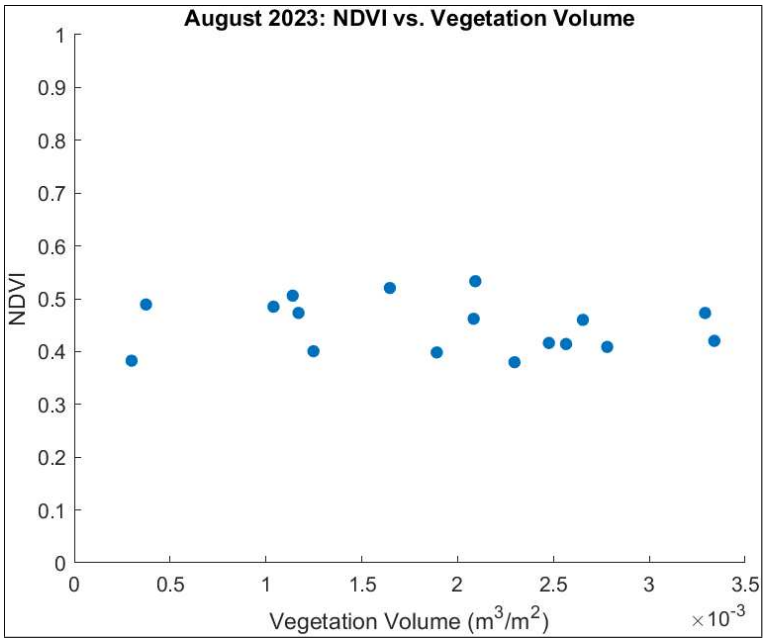

Figure 34: NDVI vs. Vegetation Volume

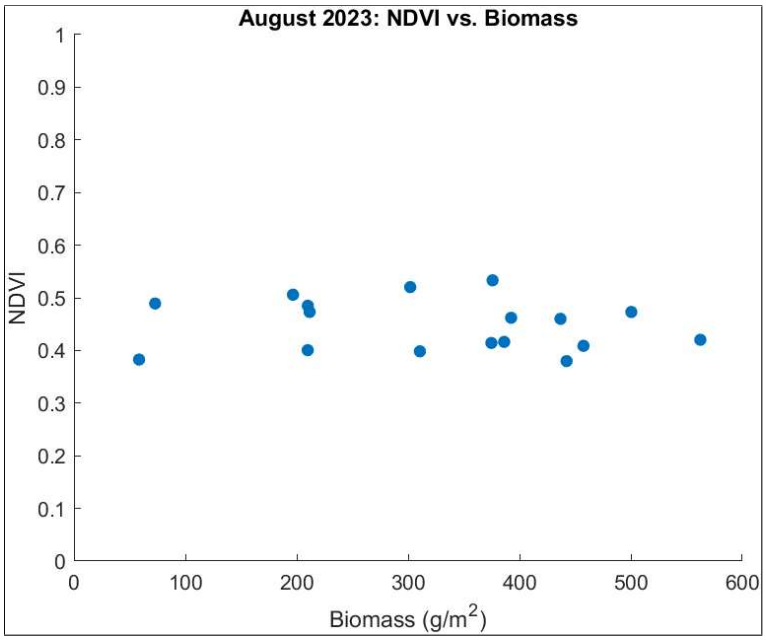

Figure 35: NDVI vs. Biomass

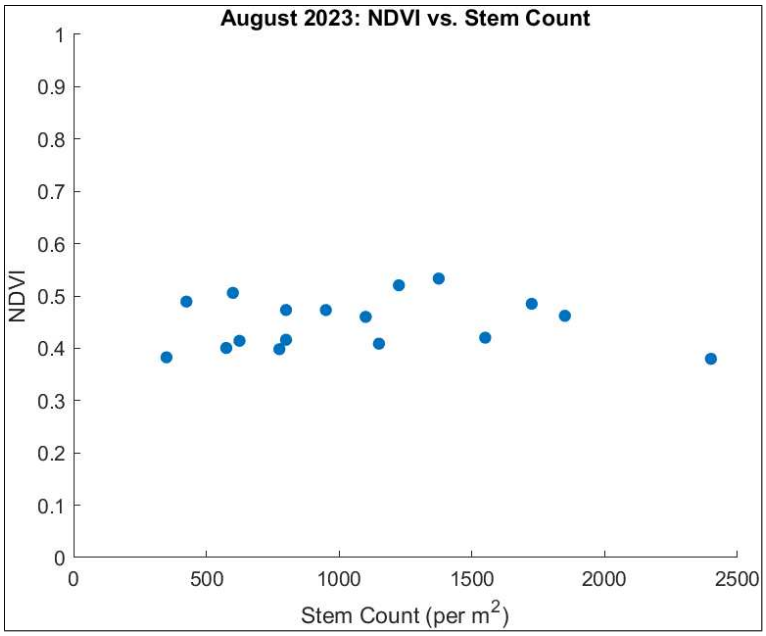

Figure 36: NDVI vs. Stem Count

A linear regression was conducted on Figs. 34, 35, and 36. The linear regression for Figs. 34, 35, and 36 are shown in Equations (38), (39), and (40), respectively.

$$\text{NDVI} = (-9 \pm 14)V + (0.47 \pm 0.03) \tag{38}$$

$$\text{NDVI} = (-0.000046 \pm 0.00009)B + (0.46 \pm 0.03) \tag{39}$$

$$\text{NDVI} = (-0.0000021 \pm 0.00002)n + (0.45 \pm 0.03) \tag{40}$$

Within uncertainty, the slopes of Figs. 34, 35, and 36 are zero which suggests there is no correlation between NDVI and vegetation abundance. Though the multiple steps in calculating plot mean NDVI were eliminated in August 2023, August 2023 also showed no correlation between mean NDVI and vegetation abundance like June 2023. As seen in Figs. 34, 35, and 36, the mean NDVI was between 0.35 and 0.55 for all vegetation abundances. For the same point in the growing season, Nardin (2021) had a NDVI range of approximately 0.4 to 0.7 and a vegetation volume of 180,000 to 380,000mm^3. The vegetation volume found by Nardin (2021) was smaller by a factor of 5 than the data captured during August 2023. However, the vegetation volume during August 2023 was smaller than June 2023 by a factor of 2 suggesting June was the peak growing season month for 2023. The difference in vegetation abundance could be attributed to different locations of study and the size range of *S. alterniflora* (Native Plant Trust, n.d.). The NDVI range for August 2023 was close and within Nardin's (2021) NDVI range. However, within the range, Nardin (2021) saw a positive correlation between NDVI and vegetation abundance. This suggests that this relationship can only be seen for smaller vegetation abundances

and there is a limit where any more increase in vegetation abundance results in the saturation of NDVI. The reason for there being no relationship could be the issue of saturation or assuming that all of the plots analyzed were homogeneous. To determine if this is the case, a threshold analysis was conducted on the August 2023 data.

Fig. 37 shows the data for control subplots separated by flight in October 2023.

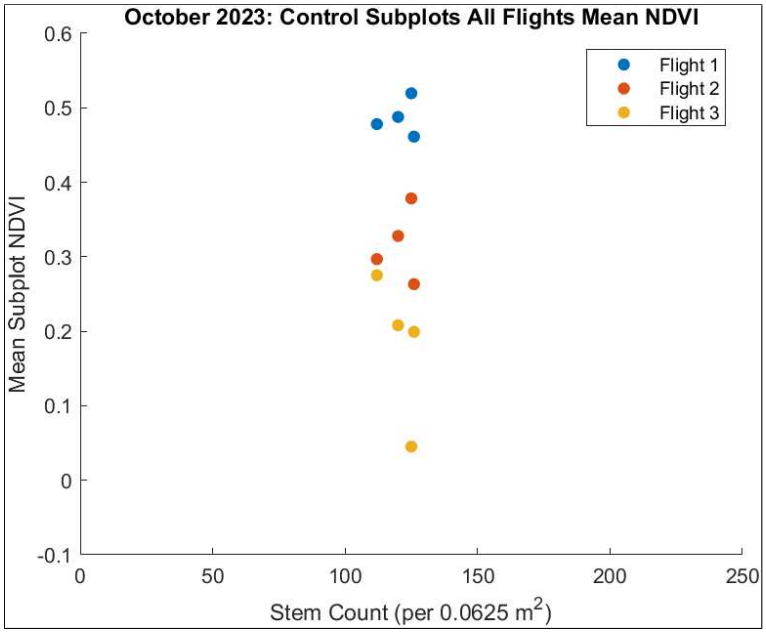

Figure 37: Control Subplots Separated by Flight

The NDVI for the control subplots in October 2023 should have not changed in Flights 1, 2, and 3 because there was no change to the *S. alterniflora* abundance. However, Fig. 37 suggests that the change in NDVI may be due to factors other than harvesting since the control subplots NDVI captured changes over the course of Flights 1, 2, and 3. As seen in August 2023, other factors that may contribute to the change in NDVI with no change in *S. alterniflora* abundance are environmental conditions.

During October 2023, there were environmental variations during the flights which included inundation and sun position. It is important to note that during Flight 1 none of the subplots were inundated. During Flight 2, the subplots were completely inundated. During Flight 3, the subplot inundation was the greatest. The average inundation during Flights 2 and 3 were recorded as $5cm$ and $19cm$, respectively. Fig. 38 shows the inundation at Plot A during Flight 3. Additionally, Flight 1 occurred at 12:00 PM, Flight 2 occurred approximately 1:00 PM, and Flight 3 occurred approximately 2:00 PM.

Figure 38: Inundation at Plot A during Flight 3 (2:00 PM)

The mean NDVI for October 2023's Flights 1, 2, and 3 were compared for each subplot. The mean NDVI should not drastically vary for the control subplots since the control subplots were not harvested. Fig. 39 shows the difference in mean NDVI calculated for all subplots during Flights 1, 2, and 3.

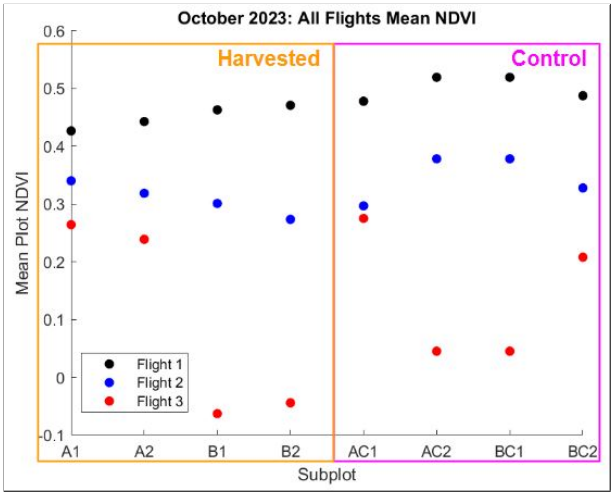

Figure 39: October 2023: All Subplots Mean NDVI All Flights

For all of the subplots, as seen in Fig. 39, Flight 1 had the greatest mean NDVI values; Flight 2 had the second greatest; and Flight 3 had the lowest. The control subplots were expected to have the same mean NDVI for all flights. This confirms the variation caused by differences in environmental conditions during flights discovered during August 2023's fieldwork.

Similar to August 2023, Beta was used for Flights 1, 2, and 3 in October 2023 to find differences between NDVI measured. Equation (37) was modified to Equation (41) to find $Beta_1$ for Flights 1 and 2 for October 2023. Equation (41) was modified to Equation (42) to find $Beta_2$ for Flights 2 and 3 for October 2023.

$$\text{Beta}_1 = \text{mean of all control subplots}(\frac{NDVI_2}{NDVI_1}) = 0.648 (41)$$

$$\text{Beta}_2 = \text{mean of all control subplots}(\frac{NDVI_3}{NDVI_2}) = 0.609 (42)$$

$Beta_1$ suggests that between Flight 1 and Flight 2, the change between NDVI calculated was approximately 35%. $Beta_2$ suggests that between Flight 2 and Flight 3, the change between NDVI calculated was approximately 39%. In addition to harvesting, $Beta_1$ and $Beta_2$ could describe the difference between the harvested subplots' variation in mean NDVI for the flights.

To further explore the relationship between NDVI and vegetation abundance, Flight 1 of October 2023 was analyzed since the flight occurred at similar environmental conditions, of sun position and tide level, as August 2022 and June and August 2023. Fig. 40 shows the NDVI of each subplot versus stem count for October 2023 with a linear fit and 95% confidence intervals.

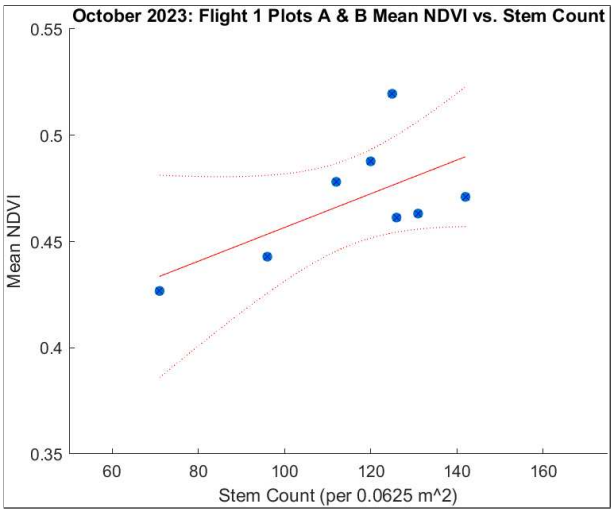

Figure 40: October 2023: Flight 1 Mean Plot NDVI vs. Stem Count

$$\text{NDVI} = (0.00079 \pm 0.0004)M + (0.38 \pm 0.05) \quad (43)$$

in which NDVI is the mean NDVI calculated per $0.0625m^2$ and M is the stem count per $0.0625m^2$. This suggests that while August 2023 did not show a relationship between mean NDVI and stem count, October 2023 did meaning that there could possibly be a relationship between mean

NDVI and vegetation abundance. While both August and October 2023 had only *S. alterniflora*, August 2023 did not show a correlation between *S. alterniflora* abundance and NDVI. The difference between August and October 2023 was the area studied in October 2023 was smaller than the area studied in August 2023. Additionally, unlike August 2023, a stem count was conducted for the entire area studied in October 2023. This indicates that the stem count conducted in the area studied in August 2023 was not representative of the entire area studied. Therefore, shoot density inhomogeneity could explain why there was a correlation found during October 2023 and not during August 2023.

4.5 Vegetation Abundance and NDVI: Harvesting

Fig. 41 is an NDVI image of Plot 6 before and after harvesting during the flights in August 2023. The harvested areas of Plot 6 are outlined near corners "B" and "D."

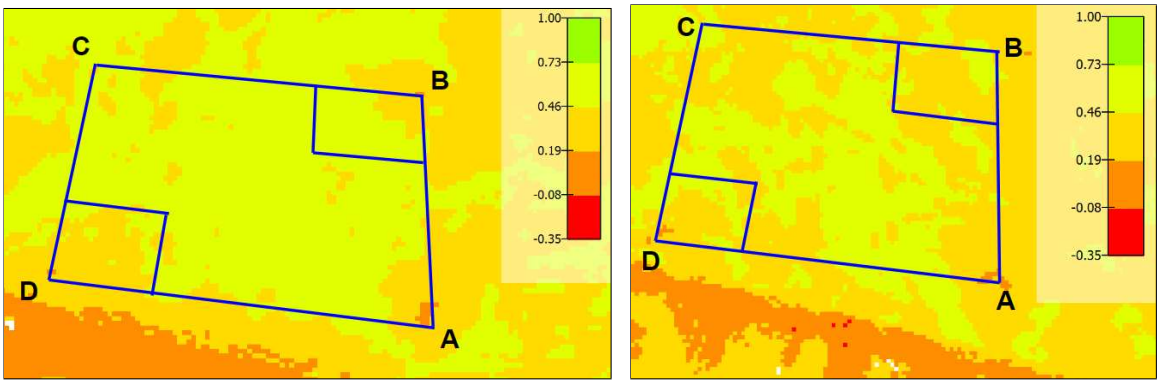

(a) Before (b) After

Figure 41: August 2023: NDVI Images Plot 6 Before and After Harvesting

After harvesting, the abundance of *S. alterniflora* decreased which was hypothesized to result in a decrease in NDVI. Fig. 41b shows a decrease in NDVI in the harvested area at corner B of Plot 6. However, there is also a decrease in NDVI in the unharvested areas of Plot 6 which suggests that the decrease in NDVI in harvested areas is not exclusively due to harvesting. To further investigate the relationship between *S. alterniflora* abundance of NDVI, the mean NDVI of the harvested areas of Plot 6 was analyzed before and after harvesting.

As seen in Table 2, the harvested areas of Plot 6's measured mean NDVI for Flights 1 and 2 were compared to a calculated mean NDVI for Flight 2 using *Beta* to determine if harvesting a portion of the plot resulted in a change in expected NDVI using *Beta* and measured NDVI. Harvesting 50% of the harvested area *S. alterniflora* after Flight 1 was hypothesized to result in a Flight 2 measured NDVI lower than a Flight 2 calculated NDVI using *Beta*.

Table 2: August 2023: Harvested Areas NDVI

Harvested Corner	Flight 1	Flight 2	
	Measured	Expected *Beta*	Measured
B	0.486	0.437	0.441
D	0.455	0.409	0.423

The measured mean NDVI for Flight 2 was greater than the calculated mean NDVI using $Beta$. The reason for the deviation from the expected result is that using $Beta$, which was the mean for all plot Flight 1 and Flight 2 ratios for August 2023, may not be representative of the environmental change of Plot 6 only. To determine if this was the reason, a $Beta_{Plot6}$ was calculated using the unharvested region, represented as a circle, of Plot 6 as seen in Fig. 21. Equation (37) was modified to Equation (44) to find $Beta_{Plot6}$. Table 3 shows the harvested areas of Plot 6's measured NDVI for Flights 1 and 2 as well as the calculated NDVI using $Beta_{Plot6}$.

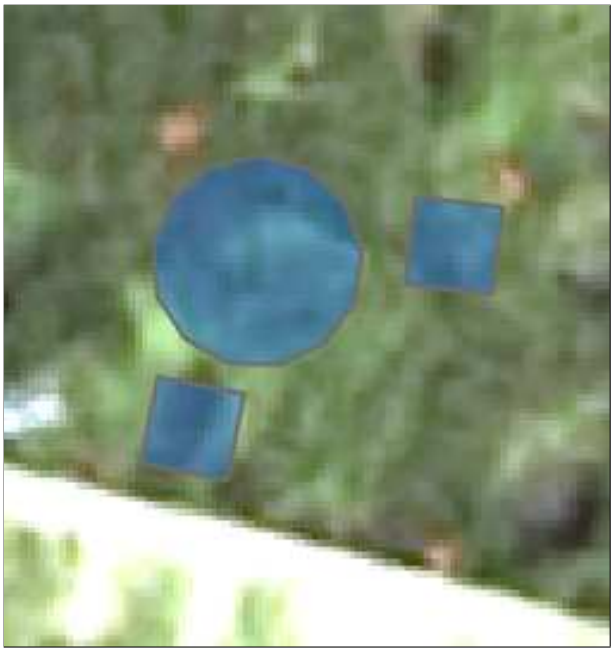

Figure 42: August 2023 (Plot 6): Portion of Unharvested Region Circled

$$\text{Beta}_{Plot6} = \text{mean of unharvested region}(\tfrac{NDVI_1}{NDVI_2}) = 0.937 (44)$$

Table 3: August 2023: Harvested Areas NDVI

Harvested Corner	Flight 1	Flight 2	
	Measured	Expected	Measured
		$Beta_{Plot6}$	
B	0.486	0.456	0.441
D	0.455	0.427	0.423

The measured mean NDVI for both harvested corners B and D during Flight 2 was less than the calculated mean NDVI using $Beta_Plot6$. This suggests that $Beta$ was not representative of the environmental changes at Plot 6. This also suggests that harvesting *S. alterniflora* decreases the NDVI measured.

Figs. 43, 44, and 45 are photos of Plots A and B before and after each harvest in October 2023.

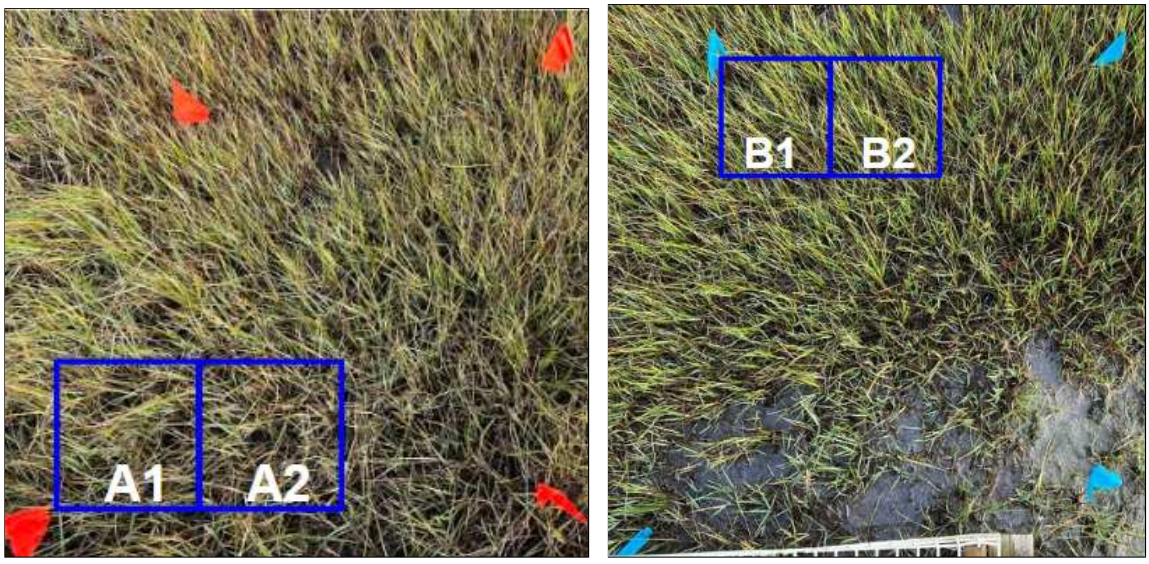

(a) Plot A (b) Plot B

Figure 43: October 2023: 100% Biomass Remaining in Harvested Subplots

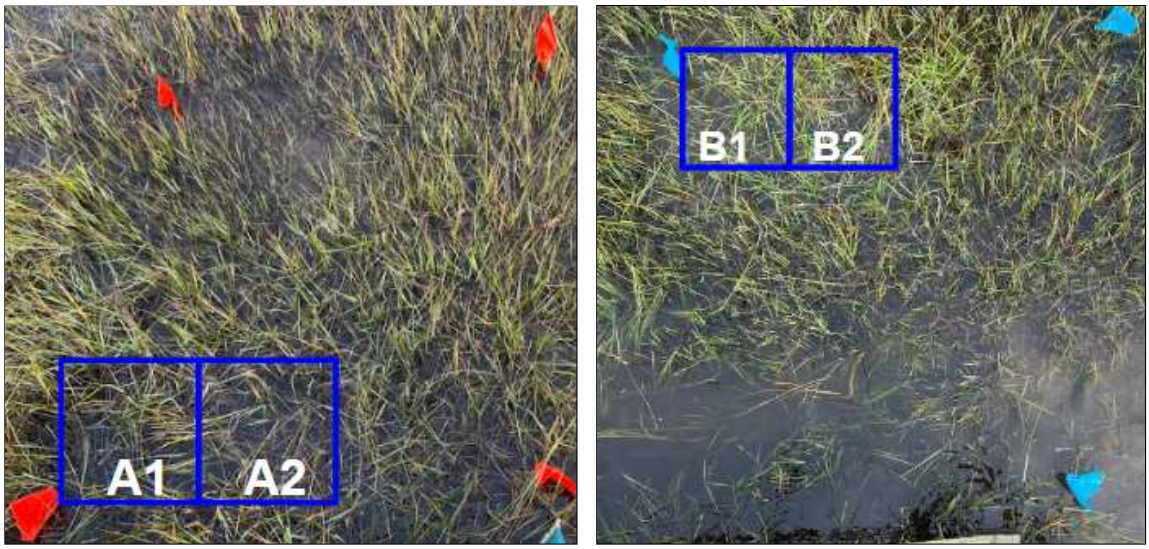

(a) Plot A (b) Plot B

Figure 44: October 2023: 50% Biomass Remaining in Harvested Subplots

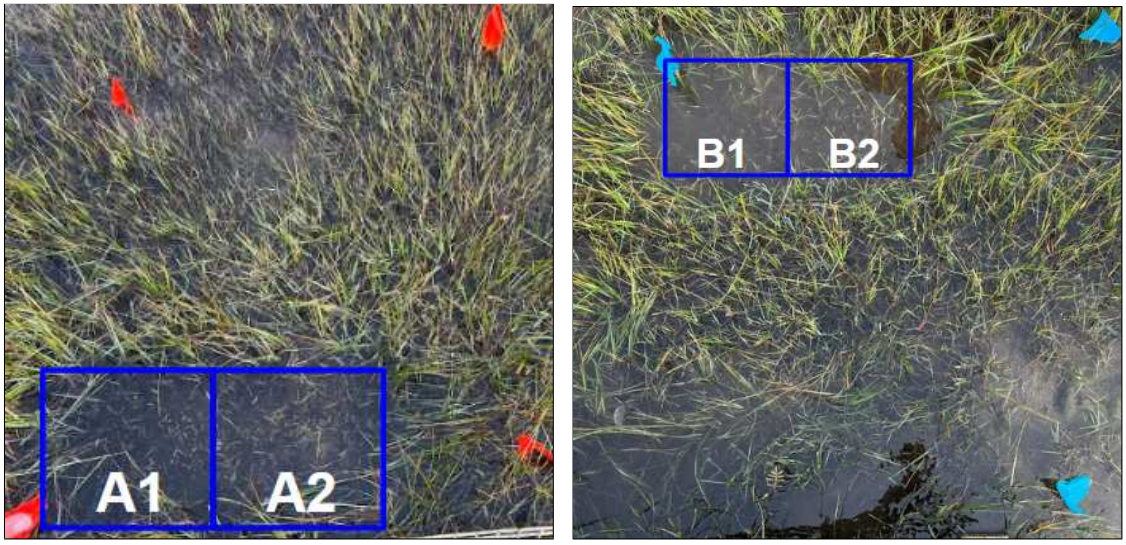

(a) Plot A (b) Plot B

Figure 45: October 2023: 0% Biomass Remaining in Harvested Subplots

As seen in Tables 4 and 5, harvested subplots A1, A2, B1, and B2's mean NDVI for Flights 1, 2, and 3 were recorded to determine if there was a change due to harvesting. $Beta_1$ and $Beta_2$ were used to calculate the expected mean NDVI of Flights 2 and 3 due to change in environmental conditions. Equation (43) was used to calculate the expected mean NDVI of Flights 2 and 3 due to harvesting to confirm whether or not the relationship between *S. alterniflora* and NDVI in Flights 2 and 3 could be described by Equation (43). While the control subplots were not harvested, the expected mean NDVI of Flights 2 and 3 using Equation (43) were calculated with

the stem count to determine whether Equation (43) was representative of all subplots. Both $Beta_1$, $Beta_2$, and harvested expected mean NDVIs were compared to the measured mean NDVI to determined if the conclusion in August 2023 of predicting mean NDVI of subsequent flights requiring the amount of *S. alterniflora* harvested and $Beta_1$ or $Beta_2$ was correct. Additionally, the harvested expected mean NDVI was used to determine whether the *S. alterniflora* abundance and NDVI relationship Flight 1 of October 2023, shown in Equation (43), and the expected mean NDVI using $Beta_1$ or $Beta_2$ was closer to the measured mean NDVI than in August 2023.

After Flight 1, 50% of *S. alterniflora* in subplots A1, A2, B1, and B2 were harvested.

Table 4: October 2023: All Subplots NDVI Flight 2

Subplot	Flight 1	Flight 2		
	Measured	Expected		Measured
		$Beta_1$	Harvested (Eqn. 13)	
A1	0.427	0.277	0.406 ±0.149	0.340
A2	0.443	0.287	0.415 ±0.160	0.319
B1	0.463	0.300	0.430 ±0.178	0.301
B2	0.471	0.305	0.433 ±0.183	0.274
AC1	0.461	0.299	0.477 ±0.236	0.263
AC2	0.478	0.310	0.466 ±0.222	0.297
BC1	0.520	0.337	0.476 ±0.235	0.378
BC2	0.488	0.316	0.472 ±0.230	0.328

For the harvested subplots in Flight 2, the calculated mean NDVI using harvesting was greater than the measured mean NDVI captured. However, both the calculated mean NDVI using harvesting and and the measured mean NDVI decreased after harvesting. This suggests that there is a positive correlation between *S. alterniflora* abundance and NDVI. However, this also suggests that the relationship between *S. alterniflora* abundance and NDVI for Flight 2 cannot be represented by Equation (43). The predicted mean NDVI using $Beta_1$ is closer to the measured mean NDVI captured than the calculated mean NDVIs using harvesting. This suggests that both harvesting and environmental conditions are required to determine the measured mean NDVI and the relationship between *S. alterniflora* abundance and NDVI.

After Flight 2, the remaining 50% of *S. alterniflora* in subplots A1, A2, B1, and B2 were harvested.

Table 5: October 2023: All Subplots NDVI Flight 3

Subplot	Flight 2	Flight 3		
	Measured	Expected		Measured
		$Beta_1$	Harvested (Eqn. 13)	
A1	0.340	0.207	0.38 ±0.05	0.264
A2	0.319	0.194	0.38 ±0.05	0.239
B1	0.301	0.183	0.38 ±0.05	-0.063
B2	0.274	0.167	0.38 ±0.05	-0.044
AC1	0.263	0.160	0.477 ±0.236	0.199
AC2	0.297	0.181	0.466 ±0.222	0.275
BC1	0.378	0.231	0.476 ±0.235	0.045
BC2	0.328	0.200	0.472 ±0.230	0.208

For the harvested subplots in Flight 3, the calculated mean NDVI using harvesting, column 4 in Table 4, is lower than the measured mean NDVI captured for Plot A and higher for Plot B. However, both the calculated mean NDVI and the measured mean NDVI decreased after harvesting. This confirms that *S. alterniflora* abundance and NDVI are positively correlated, but Equation (43) does not accurately describe the relationship between *S. alterniflora* abundance and NDVI during Flight 3. The predicted mean NDVI using $Beta_2$ is closer to the measured mean NDVI than the calculated mean NDVI using harvesting for Plot A. The converse is true for Plot B. The reason for this difference could be attributed to greater amounts of *S. alterniflora* leaves outside of, but next to, Plot A overlapping into Plot A compared to Plot B as seen in Fig. 45. The measured mean NDVI values for Plot B were negative which is the result of inundation as seen in Fig. 38. Overall, the negative relationship between harvesting and NDVI suggests that both harvesting and environmental conditions are required to determine the measured mean NDVI.

To further determine the effect of harvesting in October 2023, the harvested subplots were compared to control subplots. Fig. 46a shows the mean NDVI versus stem count for the harvested and control subplots. Fig. 46b shows the difference in mean NDVI for harvested and control subplots separated by Flights 1, 2, and 3.

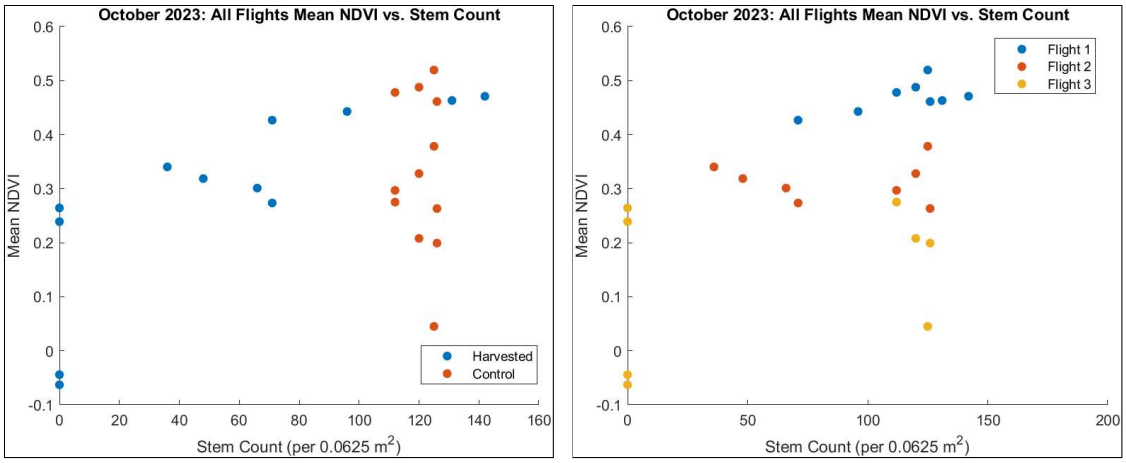

(a) Harvested vs. Control

(b) Mean NDVI vs. Stem Count

Figure 46: October 2023: Plots 3 and 5 All Flights

In Fig. 46, the difference in mean NDVI between control subplots for Flights 1 and 2 was approximately 0.15. The difference in mean NDVI between harvested sublots for Flights 1 and 2 was approximately 0.18. This suggests that harvesting did negatively impact the mean NDVI since there was a decrease in mean NDVI in the harvested subplots greater than 0.15. The difference in mean NDVI between control subplots for Flights 2 and 3 was approximately 0.2. The difference in mean NDVI between harvested sublots for Flights 1 and 2 was approximately 0.35. This suggests that harvesting did negatively impact the mean NDVI since there was a decrease in mean NDVI in the harvested subplots greater than 0.2.

5 Threshold Analysis

5.1 Deviation from Expected Relationship

In this study, the relationship between mean NDVI and stem count was hypothesized to be positively correlated. The reason for this is that as the plot stem count increases, the vegetation volume increases. The increase in vegetation volume is important because this means that there is a greater amount of vegetation reflecting and absorbing light bands which determines the NDVI captured. However, Fig. 47, stem count plotted against mean NDVI for August 2023 Flight 1, rejects this hypothesis.

The reasoning for the deviation from the expected relationship could be explained by homogeneity. The homogeneity of a plot is crucial because this study hypothesizes that only homogeneous plots could yield a correlation between NDVI and stem count.

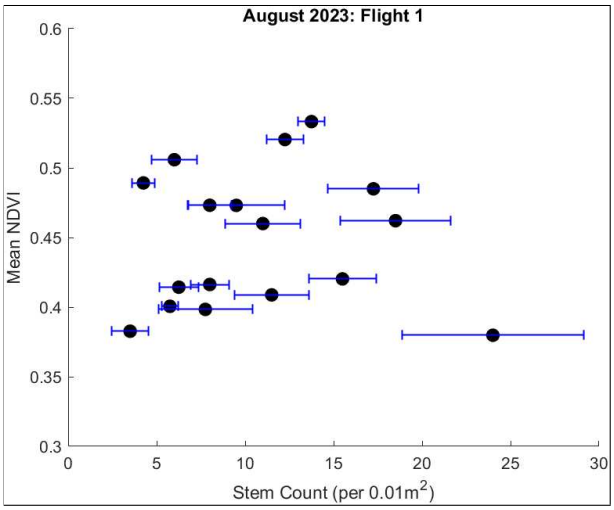

Figure 47: August 2023: Flight 1 Mean Subquadrat Stem Count vs. Mean NDVI for All Plots

Saturation could also elucidate why over a certain vegetation density, there is little to no difference in the increase in stem count and corresponding increase in mean NDVI. Previous studies observed saturation occurring when: (1) vegetation completely covers the land (Poudel et al., 2023) and at (2) high vegetation densities (Wu et al., 2023). To determine if saturation was the issue, additional thresholds of standard deviation were tested.

5.2 Determining Plot Homogeneity using Numerical Methodology

5.2.1 Defining Plot Homogeneity

For this study, homogeneous plots were defined as having a single vegetation species, ***S. alterniflora***, and uniform shoot density. Inhomogeneous plots

were characterized as having multiple vegetation species and unequal shoot density and/or the presence of bare spots.

The homogeneity of plots was determined numerically. The standard deviation of NDVI was used to numerically characterize the homogeneity of each plot. A high standard deviation within a plot postulates unequal shoot density or the presence of multiple species, or both, indicating an inhomogeneous plot. Likewise, a low standard deviation within a plot postulates uniform shoot density and the presence of a single species indicating a homogeneous plot.

5.2.2 Plot Exclusions

Plots 1-6 were excluded from this analysis due to: (1) being noted as having multiple species present during stem counts and (2) inconsistent counting methods due to different counters. The inconsistent counting method was due to counting all stems regardless of species versus only counting *S. alterniflora* stems. Fig. 48 shows a wide spread between the stem counts of Plots 1-6 as the even plots were counted by different individuals than the odd plots.

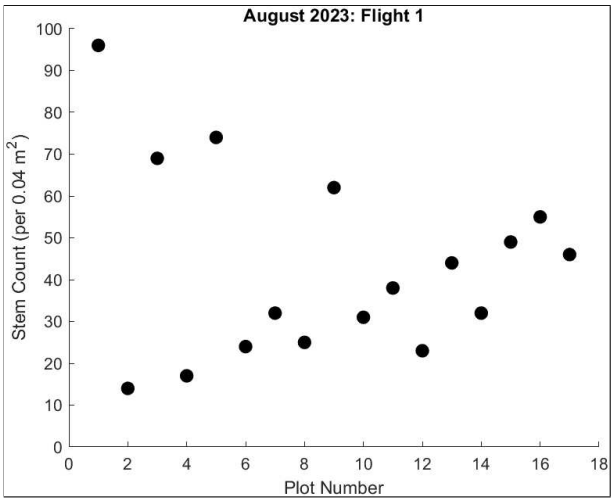

Figure 48: August 2023 (Flight 1): Inconsistent Stem Counting for Plots 1-6

5.2.3 Numerical Method for Determining Plot Homogeneity

To numerically determine homogeneous and inhomogeneous plots, different thresholds of standard deviation were chosen. The criteria for a threshold being chosen: (1) greater than the minimum standard deviation, (2) less than the maximum standard deviation, and (3) the number of plots under the threshold is not less than 5 to ensure statistical significance. The stem counts of the plots under each threshold were compared against the corresponding plot mean NDVI. The thresholds were used to determine plot

homogeneity in which plots above the threshold were considered inhomogeneous and plots below the threshold were considered homogeneous.

The final threshold, noted as being the standard deviation threshold for determining homogeneity, was determined as the standard deviation with the greatest the R^2 value with at least 5 samples left.

Fig. 49 is a plot of the mean subquadrat plot stem count vs. mean plot NDVI for Plots 7-17 during Flight 1 of August 2023. The stem counts were recorded using four 0.01 m^2 subquadrats and were not extrapolated to show the stem count of the entire 1 m^2 plot.

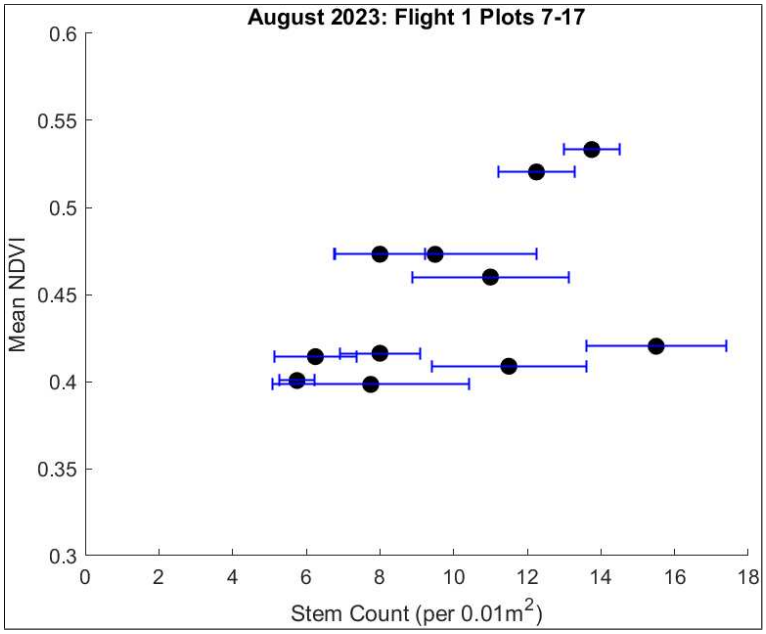

Figure 49: August 2023: Flight 1 Plots 7-17

Similar to Fig. 47, with the exclusion of plots containing multiple species, Fig. 49 shows no correlation between stem count and mean NDVI. This suggests that though Fig. 49 excludes plots containing multiple species, there could be unequal shoot density in the remaining plots.

Fig. 50 shows a standard deviation threshold of 0.05 applied to Flight 1 of August 2023. Fig. 50 is a plot of the mean subquadrat stem counts of the plots under the threshold and mean NDVI in flight 1 of August 2023.

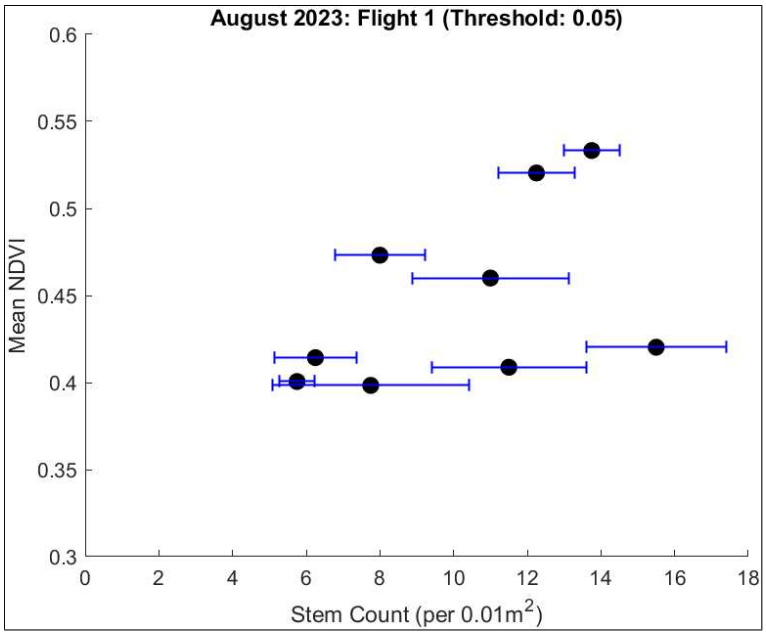

Figure 50: August 2023: Flight 1 (Threshold: 0.05)

Fig. 50 shows no correlation between mean subquadrat stem count and mean NDVI using all of the plots under the first threshold.

Fig. 51 shows a standard deviation threshold of 0.035 applied to Flight 1 of August 2023. Fig. 51 is a plot of mean subquadrat stem count and mean NDVI for the plots under the second thresholds.

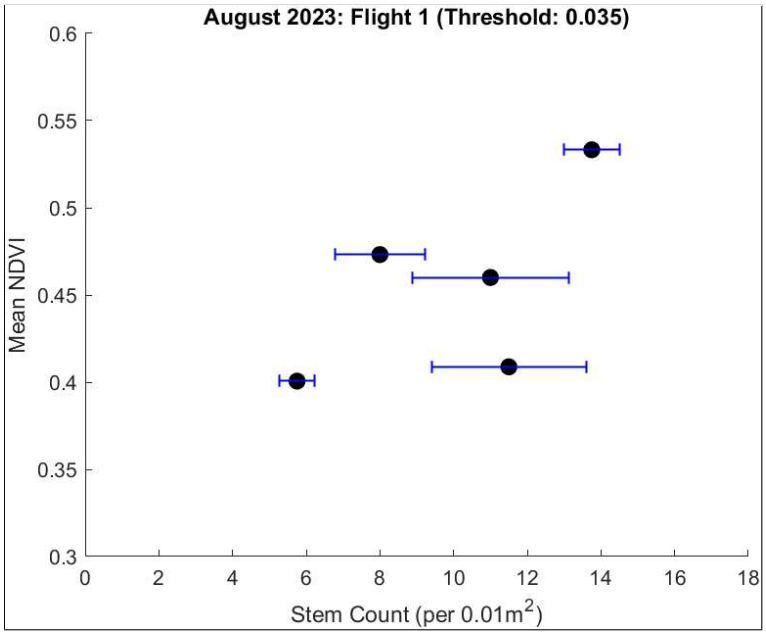

Figure 51: August 2023: Flight 1 (Threshold: 0.035)

Fig. 51 shows a positive correlation between mean subquadrat stem count and mean NDVI using all of the plots under the threshold of 0.035. This suggests that all of the plots under the threshold of 0.035 were homogeneous.

Fig. 52 shows the threshold applied to Flight 1 of August 2023 that yielded the greatest R^2 value. Since this threshold was greater than the threshold applied in Fig. 51, there were more plots that could be categorized as homogeneous in addition the ones under the threshold of Fig. 51. Fig. 52 is a plot of mean subquadrat stem count versus mean NDVI for plots under the final threshold for August 2023. The threshold shown in Fig. 52 for Flight 1 of August 2023 was a standard deviation of 0.04.

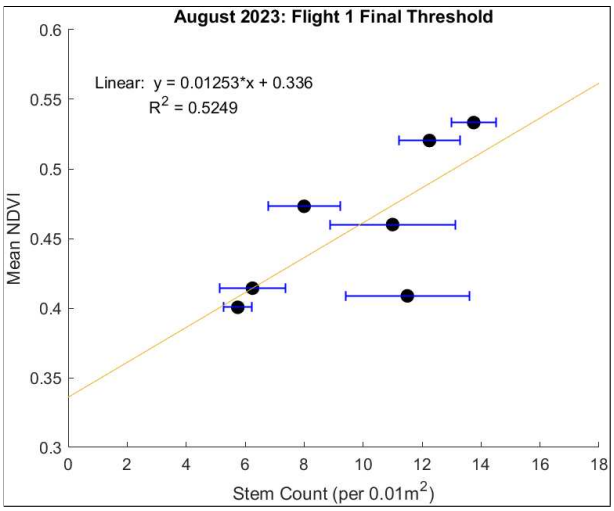

Figure 52: August 2023: Flight 1 (Threshold: 0.04)

Fig. 52 shows a positive, linear correlation for plots under the final threshold of 0.04 for August 2023. The linear regression, and standard error, of the plots under the threshold of 0.04 is shown in Equation (45).

$$y = (0.0125 \pm 0.0053)x + (0.336 \pm 0.0544) \tag{45}$$

In which, y is the predicted mean NDVI and x is the observed stem count (per 0.01 m^2). This correlation illustrates a standard deviation threshold of 0.04 characterizing the homogeneity of plots where plots with a standard deviation greater than 0.04 were inhomogeneous and plots with a standard deviation less than 0.04 were homogeneous. Figs. 49 and 50 contained plots that a threshold of 0.04 characterized as inhomogeneous, there was no correlation between stem count and mean NDVI. Conversely, Figs. 51 and 52 contained only what plot were numerically determined to be homogeneous

and both exhibit a correlation between stem count and mean NDVI. This indicates the stem count of a homogeneous plot could be extrapolated from the mean NDVI captured by multispectral images.

Table 6 is a summary of the standard deviation threshold corresponding R^2 values and number of values under the threshold. The standard deviation yielding the greatest R^2 value is highlighted in green.

Table 6: Summary of Standard Deviation Threshold and R^2 for August 2023

Standard Deviation Threshold	R^2	N
None	0.2311	11
0.06	0.2475	10
0.05	0.2261	9
0.042	0.178	8
0.04	0.5249	7
0.0395	0.4595	6
0.035	0.3946	5

5.3 Summary of Determining Plot Homogeneity using NDVI Standard Deviation

6 of the 7 plots characterized as homogeneous using the numerical method were parallel to the shore. This suggests that homogeneity is maintained in areas equidistant from the shoreline. An explanation for this is that equidistant plant zonation of *S. alterniflora* to the shoreline would subject the vegetation to similar nutrients and environmental changes (Kennish, 2002). The plots characterized as inhomogeneous by the numerical method were perpendicular to the shoreline, which suggests that homogeneity is not maintained in transects.

Table 7 shows the plots, in August 2023, determined as homogeneous or inhomogeneous using the final standard deviation threshold. Listed are the plots and corresponding stem count, mean NDVI, and NDVI standard deviation.

Table 7: Summary of Plots Characterized Numerically as Homogeneous or Inhomogeneous

Homogeneous				**Inhomogeneous**			
Plot	Stem Count	Mean NDVI	SD	Plot	Stem Count	Mean NDVI	SD
8	6.25	0.4143	0.0394	7	8	0.4163	0.0554
12	5.75	0.4006	0.0314	9	15.5	0.4203	0.0413
13	11	0.4600	0.0333	10	7.75	0.3984	0.0433
14	8	0.4732	0.0276	11	9.5	0.4731	0.0750
15	12.25	0.5204	0.0396				
16	13.75	0.5333	0.0323				
17	11.5	0.4088	0.0332				

Fig. 53 compares the homogeneous plots, determined by a standard deviation threshold of 0.04, to the inhomogeneous plots.

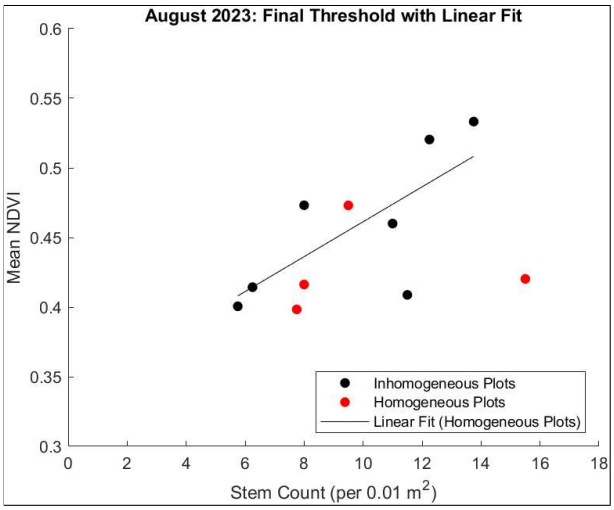

Figure 53: August 2023: Flight 1 Final Threshold Homogeneous and Inhomogenous Plot Comparison

As seen in Fig. 53, if the homogeneous plots are identified using the standard deviation threshold of 0.04, a positive, linear relationship between stem count and mean NDVI could be identified. The threshold of 0.04 does not apply in all situations will depend on multiple factors such as sun position and inundation. However, this analysis demonstrates a threshold of 0.04 for Flight 1 of August 2023 indicates that if the plots are able to be identified and separated into homogeneous and inhomogeneous categories, then mean NDVI captured using multispectral imagery could be used to determine the stem count within the surveyed area.

6 Conclusion

Field work conducted in August 2022 and June 2023 suggested that there was no correlation between *S. alterniflora* abundance and NDVI. However, the reason for no correlation was hypothesized to be due to (1) saturation, (2) species inhomogeneity, and/or (3) shoot density inhomogeneity.

To determine if the lack of relationship was due to saturation, species inhomogeneity, and shoot density inhomogeneity a threshold analysis was conducted on August 2023 data. The threshold analysis found a correlation between *S. alterniflora* abundance and NDVI for species and shoot density homogeneous plots under a NDVI standard deviation threshold of 0.04. Multiple NDVI standard deviation thresholds were tested to determine if saturation contributed to a correlation seen between *S. alterniflora* abundance and NDVI. The positive correlation between *S. alterniflora* abundance and NDVI for species and spatially homogeneous plots indicated that species and shoot density inhomogeneity contributed to no correlation seen in August 2022 and June 2023 data. Furthermore, the positive correlation between *S. alterniflora* abundance and NDVI seen after multiple NDVI standard deviation thresholds tested indicated that saturation also contributed to no correlation seen in August 2022 and June 2023 data.

To further explore the effect of shoot density inhomogeneity on the relationship between *S. alterniflora* abundance and NDVI, smaller subplots were studied in October 2023 than in August 2023. A stem count was conducted on the entire area studied in October 2023 unlike August 2023. Studying a smaller area would reduce errors introduced by heterogeneity in plant characteristics. The subplots that studied in October 2023 only contained *S. alterniflora* and showed a positive correlation between *S. alterniflora* abundance and NDVI. Unlike in the threshold analysis of August 2023 data, there were no thresholds applied on October 2023 data to obtain a correlation. This indicated that the stem count conducted in part of the area studied in August 2023 was not representative of the entire area studied. Therefore, the correlation found in October 2023 between *S. alterniflora* abundance and NDVI confirmed that shoot density inhomogeneity contributed to no correlation seen in August 2022 and June 2023 data.

Field work in August 2023 also found environmental conditions, such as inundation and sun position, effected the NDVI captured. Therefore, to accurately compare *S. alterniflora* and NDVI, field work must be conducted under similar environmental conditions between field work dates. Similarly, field work conducted in October 2023 agreed with August 2023 field work in that environmental conditions and harvesting effect the NDVI captured.

Field work conducted in August 2022 and June, August, and October 2023 found that there are limitations to using NDVI to quantify the abundance

of *S. alterniflora*. Limitations found included: (1) saturation, (2) species inhomogeneity of the area tested, (3) shoot density inhomogeneity of the area tested, and (4) environmental conditions. Furthermore, at a certain *S. alterniflora* abundance further increase of *S. alterniflora* would not be captured by NDVI due to overlapping stems not seen by the sensor; areas that contained multiple species were not representative of a relationship between *S. alterniflora* abundance and NDVI; *S. alterniflora* stem counts in a portion of the area studied could not be extrapolated over the entire area studied; and different environmental conditions would yield different NDVI measured for the same *S. alterniflora* abundance.

While NDVI can be used to determine the abundance of *S. alterniflora*, the limitations of NDVI cause the correlations to be case-specific. Therefore, NDVI should be used in small-scale controlled studies and not used as a method of quantifying large-scale correlations occurring in the natural environment. The natural environment introduces too many factors, such as species other than *S. alterniflora* and inundation, that cause NDVI measured to be inaccurate and not representative of correlations between *S. alterniflora* abundance and NDVI found in controlled environments.

7 Works Cited

Adobe. When to use low ISO settings: ISO 300 and lower. https://www.adobe.com/creativecloud/photography/hub/guides/when-to-use-low-iso-settings.html#:~:text=ISO\%20is\%20your\%20camera's\%20sensitivity,higher\%20ISO\%20means\%20more\%20sensitivity.

Bhatia, S. C. (2014). Solar Radiations. Advanced Renewable Energy Systems. https://www.sciencedirect.com/topics/engineering/solar-hour-angle#:~:text=The%20hour%20angle%20is%20the,times%201.5%20hours%20before%20noon).

Cambridge University Press & Assessment. Meaning of high noon in English. https://dictionary.cambridge.org/us/dictionary/english/high-noon.

Crosby, S.C., Angermeyer, A., Adler, J.M. et al. Spartina alterniflora Biomass Allocation and Temperature: Implications for Salt Marsh Persistence with Sea-Level Rise. Estuaries and Coasts 40, 213–223 (2017). https://doi.org/10.1007/s12237-016-0142-9.

EUMeTrain. (2010). Chapter III: Satellite Sensors and Vegetation. https://resources.eumetrain.org/data/3/36/print_3.htm#:~:text=The%20spongy%20mesophyll%20cells%20located,appears%20bright%20in%20NIR%20wavelengths.

Federal Agencies Digital Guidelines Initiative (FADGI). Term: Gain (image). https://www.digitizationguidelines.gov/term.php?term=gainimage.

González Trilla, Gabriela & Morandeira, Natalia. (2013). Allometric Scaling of Dry Weight and Leaf Area for Spartina densiflora and Spartina alterniflora in Two Southwest Atlantic Saltmarshes. Journal of Coastal Research. 29. 1373. 10.2112/JCOASTRES-D-11-00201.1.

Hill TD, Roberts BJ. Effects of seasonality and environmental gradients on Spartina alterniflora allometry and primary production. Ecol Evol. 2017; 7: 9676–9688. https://doi.org/10.1002/ece3.3494.

Kennish, Michael. (2002). Environmental threats and environmental future of estuaries. Environmental Conservation. 29. 78-107. 10.1017/S0376892902000061.

Liu, X.; Liu, H.; Datta, P.; Frey, J.; Koch, B. (2020). Mapping an Invasive Plant Spartina alterniflora by Combining an Ensemble One-Class Classification Algorithm with a Phenological NDVI Time-Series Analysis Approach in Middle Coast of Jiangsu, China. Remote Sens. 12, 4010. https://doi.org/10.3390/rs12244010.

Luhar Mitul , Nepf Heidi M. , (2011), Flow-induced reconfiguration of buoyant and flexible aquatic vegetation, Limnology and Oceanography, 56, doi:10.4319/lo.2011.56.6.2003.

Materne, M., T. Bush, M. Houck, and S. Snell. (2022). Plant Guide for smooth cordgrass (Spartina alterniflora). USDANatural Resources Conservation Service, Louisiana State Office. Baton Rouge, LA

Native Plant Trust. Spartina alterniflora - smooth cordgrass. https://gobotany.nativeplanttrust.org/species/spartina/alterniflora/.

Nardin W, Taddia Y, Quitadamo M, Vona I, Corbau C, Franchi G, Staver LW, Pellegrinelli A. (2021). Seasonality and Characterization Mapping of Restored Tidal Marsh by NDVI Imageries Coupling UAVs and Multispectral Camera. Remote Sensing. 13(21):4207. https://doi.org/10.3390/rs13214207.

NebGuide. (2017). Getting Started with Drones in Agriculture. https://extensionpubs.unl.edu/publication/g2296/html/view.

Poudel, Ananta & Shrestha, Him Lal & Mahat, Niraj & Sharma, Garima & Aryal, Sahara & Khatri, Sujan. (2023). Analyzing the Relationship Between Above Ground Biomass and Different Vegetation Indices of Chure Region of Sainamaina Municipality, Nepal. Journal of Forest and Natural Resource Management. 3. 53-67. 10.3126/jfnrm.v3i1.60149.

Sentera Support. (2022). Double 4K Multispectral - NDVI and NDRE Calculations. Doc #27063 Rev A. https://support.sentera.com/portal/api/kbArticles/280672000036465370/locale/en/attachments/bbr0j289a60820ca64408a0b201d98c0bd9fd/content?portalId=edbsndc49af6231b384d609b205eda12b95356310426ab79cfafc2949ad93d787da96\&inline=true.

Sentera Support. FieldAgent Mobile - Data Collection Best Practices. https://support.sentera.com/portal/en/kb/articles/best-practices-in-data-collection-21-10-2018#Stitched_Imagery_Maps.

Team Cropin. (2021). NDVI and its Practical Applications in Agriculture. https://www.cropin.com/blogs/ndvi-normalized-difference-vegetation-index#:~:text=NDVI%20is%20commonly%20used%20to,optimize%20irrigation%20and%20fertilization%20practices.

ThermoFisher Scientific. Exposure Times. https://www.thermofisher.com/us/en/home/life-science/cell-analysis/cell-analysis-learning-center/molecular-probes-school-of-fluorescence/imaging-basics/capturing-analyzing-your-samples/exposure-times.html#:~:text=The\%20exposure\%20time\%20is\%20how,and\%20a\%20\%E2\%80\%9Cbrighter\%E2\%80\%9D\%20image.

USDA. Normalized Difference Vegetation Index. https://ipad.fas.usda.gov/cropexplorer/Definitions/spotveg.htm

USGS. Workflow Examples: Vegetation. https://lpdaac.usgs.gov/data/get-started-data/workflow-examples/

Wenwen Liu, Wenwei Wang, Yihui Zhang, Differences in leaf traits of Spartina alterniflora between native and invaded habitats: Implication for evolution of alien species competitive ability increase, Ecological Indicators, Volume 138, 2022, 108799, ISSN 1470-160X, https://doi.org/10.1016/j.ecolind.2022.108799.

Wu, Yapeng & Wang, Wenhui & Gu, Yangyang & Zheng, Hengbiao & Yao, Xia & Zhu, Yan & Cao, Weixing & Cheng, Tao. (2023). SPSI: A Novel Composite Index for Estimating Panicle Number in Winter Wheat before Heading from UAV Multispectral Imagery. Plant Phenomics. 5. 10.34133/plantphenomics.0087.

8 Appendix

Plant ID	Biomass (g)	Frontal Area (cm^2)	Tiller Height (cm)	Number of Leaves
2-2-5-3	0.167	9.024	22.6	5
1-3-12-3	0.353	13.706	26.3	4
2-2-13-5	0.415	14.896	26.9	7
2-2-5-5	0.537	19.396	32.7	5
2-2-6-3	0.504	20.478	32.0	6
2-2-13-4	0.611	20.568	30.2	6
2-1-12-3	0.578	21.250	37.6	6
1-3-12-4	0.489	22.921	28.0	6
2-1-12-4	0.610	23.242	36.6	7
2-3-9-4	0.537	23.648	34.6	7
2-2-6-4	0.763	23.943	40.6	7
2-3-9-3	0.826	24.091	46.5	6
2-2-6-5	0.797	24.334	35.8	6
2-2-8-4	0.816	26.242	41.8	6
2-2-8-5	0.814	26.706	40.9	5
2-1-12-5	0.745	28.296	36.8	7
1-1-9-5	0.446	32.782	40.2	0
1-3-12-5	0.891	33.893	35.2	7
2-2-8-3	1.206	34.080	53.4	7
2-1-1-3	1.363	43.206	62.5	5
1-3-13-5	1.272	49.303	65.6	5
2-1-1-5	1.655	49.561	64.4	6
1-1-9-3	1.465	59.314	45.4	0
1-3-13-4	2.854	93.230	70.5	6
1-3-12-2		15.941	28.4	5
1-1-9-2		35.806	42.2	4
1-3-12-1		38.751	68.8	10
2-1-12-1		24.852	58.6	8
2-3-9-1		39.014	69.5	9
2-1-12-2		13.368	27.3	6
2-3-9-2		21.457	33.3	6
1-1-9-1		24.284	40.0	4
2-2-13-2		8.283	21.4	5
2-2-13-1		13.159	29.0	5
2-2-5-2		9.504	22.8	5
2-2-5-1		16.202	40.5	5
2-2-6-1		29.579	46.6	7
2-2-8-1		37.397	55.5	9
2-2-8-2		18.392	42.8	4
2-1-1-2		17.828	38.9	4
2-1-1-1		124.161	106.2	7
2-2-1-Large		289.956	107	9
2-2-2-Large		202.529	135	20
1-3-13-1		31.840	59.8	4
1-3-13-2		63.34	68.4	5
2-3-9-5		30.324	41.7	7
1-3-13-3		37.168	63	4
2-2-13-3		19.693	23.4	6
2-1-1-4		24.177	48.8	5
2-2-5-4		13.621	27.2	4

Table 8: August 2022 *S. alterniflora* Raw Data

Stem Count (1)	Stem Count (2)	Stem Count (3)	Stem Count (4)	MTH (cm)
1	0	2	0	22.167
0	0	3	1	23.167
17	12	17	17	16.754
11	13	18	10	22.712
29	24	14	19	22.977
9	14	21	21	22.985
9	15	19	10	35.945
11	9	9	16	37.3
17	18	10	13	28.629
7	10	10	12	29.151
23	31	14	25	37.522
23	14	16	18	33.176
20	27	34	15	30.036
23	28	22	19	24.214
24	51	26	47	21.195
35	25	37	48	36.172
41	19	34	38	31.605

Table 9: June 2023 *S. alterniflora* Raw Data

Plot	Tiller Height (cm)	Biomass (g)
3	18.1	0.254
12	16.9	0.037
10	23.6	0.1445
7	41.4	0.386
2	43.8	1.174
1	36	0.357
14	30.6	0.285

Table 10: June 2023 *S. alterniflora* Biomass Raw Data

Plot	Stem Count (1)	Stem Count (2)	Stem Count (3)	Stem Count (4)	MTH (cm)
1	23	11	36	26	26.556
2	3	4	6	1	25.136
3	15	24	11	18	21.095
4	3	4	4	6	25.512
5	11	16	25	22	28.715
6	9	3	5	7	36.556
7	11	8	7	6	45.23
8	7	7	3	8	51.111
9	21	13	13	15	38.675
10	10	9	12	0	40.867
11	6	12	16	4	47.563
12	5	5	7	6	38.8
13	7	8	13	16	40.66
14	11	9	6	6	32.45
15	10	23	15	12	31.205
16	16	13	13	13	33.05
17	17	7	12	10	40.7

Table 11: August 2023 *S. alterniflora* Raw Data

Sample	Tiller Height (cm)	Biomass (g)
1	25	0.233
2	41.25	0.524
3	22	0.114
4	17.5	0.032
5	54	0.631
6	47.5	0.530
7	9	0.065
8	32.3	0.258

Table 12: August 2023 *S. alterniflora* Biomass Raw Data

		Stem Count				MTH (cm)			
Plot	Quadrat Subplot	A1/B1	A2/B2	C1	C2	A1/B1	A2/B2	C1	C2
A	Q1+Q2+Q3	20	17	57	43	35.66	35.66	35.66	35.66
A	Q4+Q5+Q6	25	38	40	40	35.66	35.66	35.66	35.66
A	Q7+Q8+Q9	26	31	29	29	35.66	35.66	35.66	35.66
B	Q1+Q2+Q3	20	17	57	43	27.78	27.78	27.78	27.78
B	Q4+Q5+Q6	25	38	40	40	27.78	27.78	27.78	27.78
B	Q7+Q8+Q9	26	31	29	29	27.78	27.78	27.78	27.78

Table 13: October 2023 *S. alterniflora* Raw Data

Plot	Sample	MTH (cm)	Biomass (g)
A	1	33.5	0.125
A	2	30	0.199
A	3	41	0.459
A	4	24.3	0.193
A	5	49.5	0.664
B	1	30	0.110
B	2	22	0.086
B	3	32.7	0.491
B	4	29.5	0.106
B	5	24.7	0.136

Table 14: October 2023 *S. alterniflora* Biomass Raw Data

Sample	Span Length (m)	Force/Displacement (N/m)	EI (N/m^2)
1-3-12-2	0.04	752	0.0010
1-1-9-2	0.04	218.3	0.00029
1-3-12-1	0.04	5028.5	0.0067
2-1-12-1	0.04	1041.5	0.0014
2-3-9-1	0.04	5153.5	0.0069
2-1-12-2	0.04	219.4	0.00029
2-3-9-2	0.04	890	0.0012
1-1-9-1	0.04	40.6	0.000054
2-2-13-2	0.04	118	0.00016
2-2-13-1	0.04	721.1	0.00096
2-2-5-2	0.04	313.6	0.00042
2-2-5-1	0.04	660.4	0.00088
2-2-6-2	0.04	635.6	0.00085
2-2-6-1	0.04	2023.1	0.0027
2-2-8-1	0.04	3614.7	0.0048
2-2-8-2	0.04	1187.6	0.0016
2-1-1-2	0.04	764.6	0.0010
2-1-1-1	0.04	6489.6	0.0087
2-2-1-L	0.04	13086	0.017
2-2-2-L	0.04	17471	0.023

Table 15: Rigidity Calculation using Instron Output (August 2022)